Universidad Carlos III de Madrid

Nonlinear radial oscillations for hyperelastic spherical structures

Bachelor's Degree in Mechanical Engineering

Department of Continuum Mechanics and Structural Analysis

Author:

Gil Martínez, Jaime

Tutors:

Aranda-Iglesias, Damián

Vadillo, Guadalupe

Leganés, February 2016

Acknowledgements

First and foremost I would like to thank my tutors, Guadalupe and Damián, and the Department of Continuum Mechanics and Structural Analysis of the University Carlos III, for giving me the opportunity to participate on the investigation of the oscillatory behavior of hyperelastic structures. It's been a remarkable experience which I hope to continue working on because it caught my attention from the beginning and it never took its path away from my interests. Moreover, I consider it is a topic which can still be further developed and could also help the scientific community in a very important manner.

On the other hand, this work that culminates my degree couldn't have been done without my personal growth and development in life, mainly provided and triggered by my parents, who have taught me the ethics of work and commitment by which the true world is ruled, being the star that always shines, no matter what, and giving me all the necessary facilities from the beginning. To them I owe so much it couldn't be expressed in just a few words, but I must leave constancy of their actions somehow and this is my way of doing it.

I would also like to thank my best friends Carlos and Esther, who have truly being my anchors and support, and have led me through my best and worst times, have been the light at the end of the tunnel. Anything I achieve will ever have their little fingerprint on it.

Here ends the most important chapter of my life so far. This Bachelor's degree in engineering illustrates what I am and where I'm heading to. This is hard work, critical thinking, striving, and a brighter future for all that surrounds me. Here starts the most important chapter of my life…

Abstract

Throughout this paper, there has been done an extension of the work done by the department of Continuum Mechanics and Structural Analysis of the University Carlos III of Madrid, who analyzed the oscillatory behavior of cylinders [1]. However, in this case the investigation has dealt with the non-linear radial oscillations of spherical hyperelastic structures, considering free and forced oscillations of thick walled shells instead of cylinders. To do so, the model has been considered as hyperelastic, isentropic and incompressible within the framework of nonlinear elasticity. From the already mentioned field of hyperelasticity, there have been chosen two main Helmholtz free-energy functions (Mooney-Rivlin and Yeoh constitutive models). This models expose and describe the constitutive sensitivity of the oscillations and have been constantly and systematically compared. Knowing that both functions were calibrated using the same experimental data, it is eye-catching that the results will still vary in a certain degree from one model to another (see in further sections), which allows us to determine the efficacy of each model, the influence of initial conditions and other parameters, which one is more conservative, and so on.

Along with the two-model investigation, critical factors and present and future real life applications are discussed as well to leave evidence of the importance of the work developed.

Contents

List of figures

Nomenclature

λ	Stretch
λ_r	Radial stretch
λ_i	Inner stretch
λ_o	Outer stretch
λ_θ	Circumferential stretch along direction 1
λ_ϕ	Circumferential stretch along direction 2
r	Deformed coordinate for generic radius
R	Undeformed coordinate for generic radius
dr	Differential deformed generic radius
dR	Differential undeformed generic radius
$d\theta$	Differential circumferential angle 1
$d\phi$	Differential circumferential angle 2
σ_r	Cauchy radial stress
σ_θ	Cauchy circumferential stress 1
σ_ϕ	Cauchy circumferential stress 2
$\ddot{r}$	Generic point acceleration
ρ	Material density
τ	Dimensionless time
t_0	Dimensionless time variable
$\bar{\sigma}$	Dimensionless stress
C_{10}	Material constant parameter
$\bar{R}$	Dimensionless undeformed generic radius
R_i	Inner undeformed radius
R_o	Outer undeformed radius
$\bar{r}$	Dimensionless deformed generic radius
ψ	Helmholtz free-energy function
$\bar{\psi}$	Dimensionless Helmholtz free-energy function
$\dot{\lambda}$	Radial stretch derivative, radial velocity
$\ddot{\lambda}$	Radial stretch second derivative, radial acceleration
$\Delta\bar{P}$	Dimensionless pressure difference term
μ	Thickness parameter

C	Initial conditions parameter
α	Mooney-Rivlin material constant 1
β	Mooney-Rivlin material constant 2
I_1	First invariant
I_2	Second invariant
C_1	Yeoh material constant 1
C_2	Yeoh material constant 2
C_3	Yeoh material constant 3
K	Kinetic energy term
Π_{ext}	External forces term
Π_{int}	Internal elastic stored energy term
T	Period

Chapter 1: Introduction and importance of the work

Aneurysms are a type of disease related with blood arteries. They consist on the inflation of blood vessels due to the weakness of the wall at a certain spot (see figure 1). Aneurysms can be caused by (high) internal blood pressure or some other factors and there are some conditions, such as gender or smoking, that may aggravate the possibility of rupture. They can be formed in any body blood vessel, but only brain aneurysms can lead to serious medical conditions. Moreover, brain aneurysms are a particular case of aneurysms because they adopt a spherical shape instead of a bulged cylinder (as in any other aneurysm). In fact, if the bulging sphere strokes, it triggers an internal hemorrhage that causes brain damage and possibly death [2,3,4,5,6]. In this investigation, we have focused on the modeling of a hyperelastic sphere that likens brain aneurysms behavior. It has been subjected to free and forced radial oscillations, as will be detailed in further sections.

This investigation has therefore an extremely interesting feature carried along that may not surface to the reader's mind unless it is previously expressed. It combines two of the most powerful study branches that the human being has developed and learned knowledge about through history: physiology and engineering.

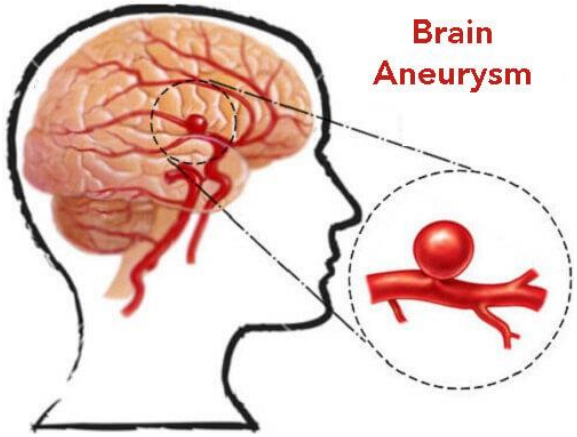

Figure 2. Aneurysm on brain vessel representation. It likens a hyperelastic spherical structure.

Then, to approach the investigation correctly, we need to see the context on which the study will be carried on. To effectively disclose aneurysms' behavior, it is necessary to claim a large deformations framework, which is typically not included in engineering bachelor degrees' programs. Therefore, it requires familiarity within a context of non-linear hyperelasticity, an extension of the knowledge commonly imparted on strength of materials. This large deformations background will allow to approach real life conditions and consequently give reliability to the results. And finally, it is also remarkable to say that due to the nature of the problem we will be situated within a situation of dynamic motion, instead of static conditions, a very common assumption made during the degree.

The investigation will be focused on mathematically modeling the aneurysm and describing the type of motion that the spherical structure yields in two different conditions: free and forced radial oscillations. Moreover, there will also be two material models investigated, to expose the constitutive sensitivity of the problem. This two models and their dependence to different parameters will be analyzed in each type of oscillation to give conclusive and precise results that open the door to future investigations.

1.1 Objectives

The purpose of the investigation will be to determine how hyperelastic spherical structures behave within the contexts of free and forced oscillations. However, there exist intermediate goals necessary to achieve before completion, such as

- Understanding hyperelastic materials: the models that conduct its behavior, the form that the incompressibility condition takes or the implications regarding deformation that they have.
- Being able to mathematically develop the equations of the problem: as will be observed in further sections, starting from a linear momentum balance we derive the equations that will help us to obtain the desired results.
- Utilizing adequate programming languages: in this particular case, *Mathematica* [7] will be the program used to plot the necessary graphs and resolve the equations needed.
- Identifying boundary conditions and limits to the problem: They are probably the most critical factor in order to demonstrate credibility and correctness. Isotropy, incompressibility, time-independent applied pressures or valid range of oscillations are some of the examples.

and ultimate goals to reach after obtaining the oscillatory behavior, as anticipated before. Here is the breakdown, point by point

- Determine how different situations affect the problem: regarding free or forced periodic motions.
- Analyze constitutive sensitivity: to determine the sensitivity depending of the hyperelastic model selected, which will play a very important role.
- Check variables influence: to see how thickness or total energy affect very different parameters such as amplitude, period or velocity influence.
- Obtain relevant conclusions about the results: being able to critically analyze what the results tell us and why they do is the most important task. It determines whether the work developed is useful and should be continued or it is irrelevant instead.

Chapter 2: Problem formulation

The purpose of this section is to derive the differential equations that govern the large amplitude oscillations problem presented. The material used will be a hyperelastic, incompressible, isotropic and thick spherical shell within the framework of finite non-linear elasticity, where radially symmetric motion will be considered. Further details of mathematical derivation can be found in the seminal works of Knowles [8,9].

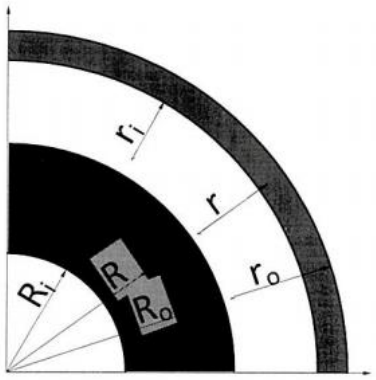

Figure 3. Reference (undeformed) and motion (deformed) coordinates.

Assuming a reference configuration where the spherical undeformed structure is set, let (R, Θ, Φ) be the polar coordinates of the sphere. Then, assuming that the symmetry will prolong in time when oscillations occur, let (r, θ, φ) be the parameters that define the dynamic coordinates (the coordinates used from now on) for the deformed sphere throughout its motion, where

$$r = f(R,t)R; \qquad \theta = \Theta; \qquad \varphi = \Phi; \tag{1}$$

as shown in figure 2. Note that subscripts *i* and *o* will account for the inner and outer particularizations of the variable throughout the whole investigation and no subscript will stand for a generic value of the corresponding variable. The balance of linear momentum applied on a differential volume

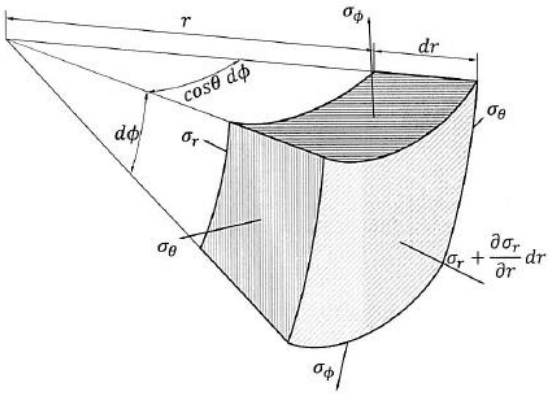

Figure 4. Balance of linear momentum.

leads to the following relation

$$(\sigma_r + d\sigma_r)(r + dr)^2 cos\theta d\phi d\phi - \sigma_r r^2 cos\theta d\phi d\phi - 2\sigma_\theta r d\phi dr sin\left(\frac{cos\theta d\phi}{2}\right) - 2\sigma_\phi r cos\theta d\phi dr sin\left(\frac{d\phi}{2}\right) = \rho r^2 cos\theta d\phi d\phi dr\ddot{r} \quad (2)$$

where $\sigma_i = f(r,t)$ represent Cauchy stresses on the subscript indicated direction. Applying the following conditions

- Small angles: $cosx = 1, sinx = x$
- σ_r dependence to only one variable: $d\sigma_r = \frac{\partial \sigma_r}{\partial r}\, dr$
- Spherical symmetry: $d\theta = d\phi;\ \ \sigma_\theta = \sigma_\phi$

we obtain

$$\frac{\partial \sigma_r}{\partial r} + 2\,\frac{(\sigma_r - \sigma_\theta)}{r} = \rho\ddot{r} \quad (3)$$

This initial equation will be derived and modified in order to find a more useful expression that explains the sphere's motion in terms of desired variables, such as stretch or thickness. Notice that for the sign criteria there have been chosen as positive outwards or expansive directions and as negative inwards or compressive directions. Therefore, acceleration will be positive when the sphere expands and negative when it compresses. This will have significant importance on further sections, when phase diagrams are analyzed.

In order to verify equations in terms of units and to develop systematic experiments, it is very useful to introduce a set of dimensionless variables. For this particular case, they will be

$$\tau = \frac{t}{t_0}; \qquad \bar{\sigma} = \frac{\sigma}{C_{10}}; \qquad \bar{R} = \frac{R}{R_i}; \qquad \bar{r} = \frac{r}{R_i} \quad (4)$$

where C_{10} is a material constant and t_0 the dimensionless time value. Both will be further discussed in appendix A. From now on, all dimensionless parameters (except for τ, dimensionless time) will be denoted with a bar above it for the sake of clarity and uniformity, as shown. Plugging the values in equation (3) and rearranging terms yields

$$\frac{\partial \bar{\sigma}_r}{\partial \bar{r}} + 2\,\frac{(\bar{\sigma}_r - \bar{\sigma}_\theta)}{\bar{r}} = \ddot{\bar{r}} \quad (5)$$

where $\ddot{\bar{r}}$ represents the differentiation with respect to the dimensionless variable of time previously defined.

Let us then define the stretches as

$$\lambda_r = \frac{\partial \bar{r}}{\partial \bar{R}} \; ; \qquad \lambda_\theta = \lambda_\phi = \frac{\bar{r}}{\bar{R}} = \lambda \tag{6}$$

where recall that *r* stands for the deformed radius and *R* for the undeformed or reference radius. Then, the incompressibility condition for hyperelastic materials yields $\lambda_r \lambda^2 = 1$. Integrating from the inner radius $\bar{r}_i$, $\bar{R}_i$ to a generic point in the spherical wall $\bar{r}, \bar{R}$ we find

$$\lambda\,(\bar{r}, \tau) = \sqrt[3]{\frac{(\bar{r}_i^{\,3} - 1)}{\bar{R}^3} + 1} \tag{7}$$

from which we can obtain its derivatives with respect to $\bar{r}$ and τ. The first

$$\frac{\partial \lambda}{\partial \bar{r}} = -\frac{\lambda^3 - 1}{\bar{R}} \tag{8}$$

allows to change the derivation variables in equation (5)

$$\frac{\partial \bar{\sigma}_r}{\partial \lambda} + 2\,\frac{(\bar{\sigma}_r - \bar{\sigma}_\theta)}{\bar{r}} \frac{\bar{R}}{1 - \lambda^3} = \ddot{\bar{r}} \frac{\bar{R}}{1 - \lambda^3} \tag{9}$$

so that it becomes

$$\frac{\partial \bar{\sigma}_r}{\partial \lambda} + 2\,\frac{(\bar{\sigma}_r - \bar{\sigma}_\theta)}{\lambda\,(1 - \lambda^3)} = \ddot{\lambda} \frac{\bar{R}}{1 - \lambda^3} \tag{10}$$

where now the equation depends on the stretch, λ, the stresses, σ, and the wall's acceleration, $\ddot{\lambda}$. The acceleration can precisely be obtained from the second derivative of equation (7) (see in appendix B)

$$\ddot{\lambda} = \frac{\lambda^3 - 1}{\lambda_i^{\,3} - 1} \left[\frac{2\lambda_i \dot{\lambda_i}^{\,2} + \lambda_i^{\,2} \ddot{\lambda_i}}{\lambda^2} - \frac{2\lambda_i^{\,4} \dot{\lambda_i}^{\,2}}{\lambda_i^{\,3} - 1} \frac{\lambda^3 - 1}{\lambda^5} \right] \tag{11}$$

Now, the incompressibility condition allows to rewrite the equation $\frac{\partial \bar{\sigma}_r}{\partial \bar{r}} + 2\,\frac{(\bar{\sigma}_r - \bar{\sigma}_\theta)}{\bar{r}} = \ddot{\bar{r}}$ as a partial differential equation replacing the independent variable $\bar{r}$ by λ

$$\frac{\partial \bar{\sigma}_r}{\partial \lambda} + 2\frac{(\bar{\sigma}_r - \bar{\sigma}_\theta)}{\lambda \cdot (1-\lambda^3)} = -\frac{(2\lambda_i \dot{\lambda_\iota}^2 + {\lambda_i}^2 \ddot{\lambda_\iota})}{\lambda^2(\lambda^3-1)} + \frac{2{\lambda_i}^4 \dot{\lambda_\iota}^2}{\lambda^5({\lambda_i}^3-1)} \tag{12}$$

Moreover, according to Ogden [10], for an incompressible spherical shell we have

$$\overline{\sigma_r} - \overline{\sigma_\theta} = -\frac{1}{2}\,\lambda\,\frac{\partial \bar{\psi}}{\partial \lambda} \tag{13}$$

where the dimensionless strain-energy is defined as $\bar{\psi} = \frac{\psi}{\mathrm{C10}}$. The specific form of ψ will be defined in section 3. Now, we insert equation (13) on equation (12) and integrate over the thickness

$$\int_{-\bar{P}_\iota}^{-\overline{P_o}} \partial \bar{\sigma}_r = \int_{\lambda_i}^{\lambda_o} \frac{\partial \bar{\psi}}{\partial \lambda}\frac{\partial \lambda}{(\lambda^3-1)} - \left(2\lambda_i \dot{\lambda_\iota}^2 + {\lambda_i}^2 \ddot{\lambda_\iota}\right)\int_{\lambda_i}^{\lambda_o} \frac{\partial \lambda}{\lambda^2 \cdot (\lambda^3-1)} + \frac{2{\lambda_i}^4 \dot{\lambda_\iota}^2}{({\lambda_i}^3-1)}\int_{\lambda_i}^{\lambda_o} \lambda^{-5} \tag{14}$$

where the time independent external pressures acting on both the internal and external surfaces of the shell are defined as $\bar{P}_i$ and $\bar{P}_o$ respectively. Then, the integral results in

$$\begin{aligned}\overline{\Delta P} = (\overline{P_i} - \overline{P_o}) = \int_{\lambda_i}^{\lambda_o} \frac{\partial \bar{\psi}}{\partial \lambda}\frac{\partial \lambda}{(\lambda^3-1)} + \left(1 - \frac{\lambda_i}{\sqrt[3]{\mu + {\lambda_i}^3}}\right)\lambda_i\,\ddot{\lambda_i} \\ + \dot{\lambda_i}^2\left(\frac{3}{2} - \frac{2\lambda_i}{\sqrt[3]{\mu + {\lambda_i}^3}} + \frac{{\lambda_i}^4}{2\cdot(\mu + {\lambda_i}^3)\sqrt[3]{\mu + {\lambda_i}^3}}\right)\end{aligned} \tag{15}$$

which is a second-order ordinary differential equation in λ_i. Note that a new term μ has been defined. It is the thickness parameter

$$\mu = \frac{{R_o}^3}{{R_i}^3} - 1 \tag{16}$$

defined by particularizing equation (7) for $\lambda = \lambda_o$ and $\bar{R} = \overline{R_o}$ and rearranging some terms. Note that as the thickness parameter increases, the thickness of the shell increases as well, which will be very useful in coming sections.

Then, upon multiplication by $2 \cdot {\lambda_i}^2$ expression (15) can be rewritten as

$$P_{ext} = P_{int} + \frac{d}{d\lambda_i}\,[K] \tag{17}$$

where

$$P_{ext} = \ 2\,(\overline{\Delta P})\,{\lambda_i}^2 \tag{18}$$

$$P_{int} = \left(2\int_{\lambda_i}^{\lambda_o} \frac{\partial \bar{\psi}}{\partial \lambda}\frac{\partial \lambda}{(\lambda^3 - 1)}\right){\lambda_i}^2 \tag{19}$$

$$K = \left[\left(1 - \frac{\lambda_i}{\sqrt[3]{\mu + {\lambda_i}^3}}\right){\lambda_i}^2{\dot{\lambda}_i}^2\right] \tag{20}$$

P_{ext} stands for the external forces, P_{int} for the elastic stored energy, and *K* for the kinetic energy. This equation can be integrated in time, this is from the undeformed configuration to a generic deformed estate, to obtain the final energy balance of the problem

$$C = \ K + \ \Pi_{int} \ + \ \Pi_{ext} \tag{21}$$

where C is the constant of integration. The constant of integration will represent in the problem the total energy estate of the system, which is naturally defined as the sum of all the energies. Kinetic energy, K, has already been defined in equation (20) but the remaining energies are defined as

$$\Pi_{int} \ = \ \int_1^{\lambda_i}\left(2\int_{\lambda_i}^{\lambda_o} \frac{\partial \bar{\psi}}{\partial \lambda}\frac{\partial \lambda}{(\lambda^3 - 1)}\right){\lambda_i}^2 \cdot d\lambda_i \tag{22}$$

$$\Pi_{ext} \ = \ -\int_1^{\lambda_i} 2\,(\overline{\Delta P})\,{\lambda_i}^2 \tag{23}$$

Recall that equation (20) stands for the kinetic energy, but potential energy splits into (22) elastic stored energy, Π_{int}, and (23) the work done by external forces, Π_{ext}. Let us now analyze the importance and dependencies of every term.

Internal stored energy (22) contains the strain-energy function and therefore determines the behavior (stretch) based on the chosen material (implied by $\bar{\psi}$) and also on the geometry (thickness). Therefore, its variation provides a very useful path to see the influence of different constitutive models (see next section), isolating its effect from any other parameter. On every section, we will distinguish between the two different strain energy functions to demonstrate its relevance.

External pressures term (23) deals with the role played by external forces. It allows to differentiate between the two main dynamic behaviors investigated (free and forced oscillations), once the initial conditions have been correctly set. It depends on the stretch and the pressure values. This is another big topic to be discussed throughout the document and along with the

models (the two different strain-energy functions), it will conform the ground basis on which the problem settles.

The kinetic energy term (20) deals with the dynamics of the problem and it is the only velocity-dependent term, and because oscillations are studied, the most critical factor. This term depends on the dimensionless time, the stretch, and the thickness parameter.

Finally, C is the initial energy in the material due to $\lambda_i(0)$ or $\dot{\lambda}_i(0)$.

The relationship between the velocity of deformation and all the different energies can also be established. It is what we call phase diagrams (see equation 24) These diagrams come from plotting radial velocity versus radial stretch, so in equation (21) we can solve for the velocity and obtain the function depending on the stretch that will provide very useful information to the investigation

$$\dot{\lambda}_i = \sqrt{\frac{C - \Pi_{ext} - \Pi_{int}}{\lambda_i^2 \left(1 - \frac{\lambda_i}{\sqrt[3]{\mu + \lambda_i^3}}\right)}} \tag{24}$$

Note that for the motion to be periodic, there must be at least two points where the motion is reversed (from expansion to compression and vice versa) and velocity equals zero, which translates into two real roots for equation (24). Therefore, the numerator of the function $C - \Pi_{ext} - \Pi_{int}$ must at least have these two roots, say a, b. Moreover, for the motion to be periodic, the corresponding phase curve must be a closed loop in the $(\dot{\lambda}, \lambda)$ plane.

Regarding the temporal behavior of the circumferential stretch, a second integration of equation (16) between the roots yields the last term to be taken into account, the period

$$T = 2\int_a^b \frac{d\lambda_i}{\dot{\lambda}_i(\lambda_i)} \tag{25}$$

Chapter 3: Constitutive modelling

As anticipated, there are two Helmholtz free-energy functions taken in order to describe and expose the constitutive sensitivity of the oscillatory behavior of the thick-walled shell. The idea is to study the different functional dependencies of λ on ψ. These are Mooney-Rivlin and Yeoh constitutive models.

3.1 Mooney-Rivlin model

Considering a Mooney-Rivlin material, the Helmholtz free-energy comes down to be, by definition:

$$\psi = \frac{1}{2}\,\alpha\,(I_1 - 3) + \frac{1}{2}\,\beta\,(I_2 - 3) \tag{26}$$

where α, β are material constants whose values are defined in appendix A, and I_1, I_2 invariants of the Green strain tensor. By definition, $I_1 = \sum_{i=r,\theta,\phi} {\lambda_i}^2$ and $I_2 = \sum_{i,j=r,\theta,\phi} {\lambda_i}^2 {\lambda_j}^2 \;\; \forall\, i \neq j$. Recalling incompressibility condition $\lambda_r \lambda_\theta \lambda_\phi = 1$ and spherical symmetry $\lambda_\theta = \lambda_\phi = \lambda$, we can therefore establish that

$$I_1 = \lambda^{-4} + 2\,\lambda^{2} \tag{27}$$

$$I_2 = \lambda^{4} + 2\,\lambda^{-2} \tag{28}$$

Introducing the dimensionless strain-energy function value we provide the final expression for a Mooney-Rivlin Helmholtz free-energy function, that can be written as

$$\bar{\psi} = \frac{1}{2\,C_{10}}\,\alpha\,(\lambda^{-4} + 2\,\lambda^{2} - 3) + \frac{1}{2\,C_{10}}\,\beta\,(\lambda^{4} + 2\,\lambda^{-2} - 3) \tag{29}$$

so then the final storage energy term (22) for this material will be

$$\begin{aligned} \Pi_{int}\,(\lambda_i, \mu) = {} & \frac{\alpha}{c_{10}}\left(\frac{1}{\lambda} - 2 * \lambda^2 - \mu + \sqrt[3]{\frac{\mu+1}{\mu+\lambda^3}} * (2 * \lambda^3 + \mu - 1)\right) \\ & + \frac{\beta}{c_{10}}\left(\lambda^4 - 2 * \lambda - \mu - \sqrt[3]{\frac{\mu+\lambda^3}{\mu+1}} * (\lambda^3 - \mu - 2\right) \end{aligned} \tag{30}$$

Note that as equation (22) is integrated, the function depends on λ and μ.

3.2 Yeoh model

Starting off with a similar expression to Mooney-Rivlin's model:

$$\psi = C_1 (I_1 - 3) + C_2 (I_1 - 3)^2 + C_3 (I_1 - 3)^3 \tag{31}$$

where C_1, C_2, C_3 are also constant materials equivalent to those mentioned in Mooney-Rivlin's section. These are also defined in appendix C for completeness. Knowing that the invariants are naturally equal for both cases (they are independent of the chosen model) and using the same symmetry reasoning as in Mooney-Rivlin, the Yeoh Helmholtz free-energy function turns out to be:

$$\bar{\psi} = \frac{C_1}{C_{10}} (\lambda^{-4} + 2\lambda^2 - 3) + \frac{C_2}{C_{10}} (\lambda^{-4} + 2\lambda^2 - 3)^2 + \frac{C_3}{C_{10}} (\lambda^{-4} + 2\lambda^2 - 3)^3 \tag{32}$$

and after time integration of equation (22) for this particular case we find for a Yeoh material

$$\Pi_{int} (\lambda_i, \mu) = 2\frac{C_1}{c_{10}} * (A) + 2\frac{C_2}{c_{10}} * (B) + 6\frac{C_3}{c_{10}} * (C) \tag{33}$$

where A, B, C are extremely long terms that will be omitted and detailed in appendix C as well for the sake of brevity.

All constants used were determined by Bucchi and Hearn [11,12] in a model calibration that used the same set of experimental results. Note that Yeoh materials have higher order I_1 and no I_2. According to Boyce and Arruda [13] and Selvadurai [14], this seizes the response of hyperelastic materials in large deformations problems.

Chapter 4: Free oscillations

In this section we will set $\Delta\bar{P}$ equal to zero as the boundary condition, in order to cause free oscillations of the sphere. Then, the whole external pressure term (23) becomes null, with severe implications on phase diagrams (24), whose equation will now take the following form

$$\dot{\lambda_i} = \sqrt{\frac{C - \Pi_{int}}{\lambda_i^2\left(1 - \frac{\lambda_i}{\sqrt[3]{\mu + \lambda_i^3}}\right)}} \tag{34}$$

Velocity equation (or phase diagram equation) precisely describes the motion depending on different parameters. Specifically in this section, it will only depend on three terms: the internal energy (Π_{int}), the total energy constant (C), and the kinetic energy remaining term (from which $\dot{\lambda_i}$ was solved, the denominator). As anticipated, and due to the nature of the phase diagram equation form, the numerator will be a critical factor because it delimits the zeroes of the velocity function, and so it deserves a broad study of its own (see figure 5 (a)). When $C = \Pi_{int}$, velocity becomes zero, and because C is a constant we can simply select C arbitrary values for descriptive purposes and see when the function equalizes the total energy.

Once $\Delta\bar{P} = 0$ is set, we proceed to investigate the roles that all the different parameters play in the phase diagram. Specifically, we will investigate the influence of the thickness and the total energy constant within each strain-energy function case. Let us start by looking at the shape that the function takes and at the phase diagrams to approach the problem's understanding.

4.1 Mooney-Rivlin model

Recall that Π_{int} depends on the stretch and the thickness parameter, μ. In order to study the oscillations we need to isolate the effect of the stretch, so we must choose one thickness value as a reference and work with the stretch dependency. Recall that $\mu = \frac{{R_o}^3}{{R_i}^3} - 1$ so we can set it equal to one for simplicity, implying that the corresponding values of the internal and external radii are proper. Indeed, for $\bar{R_i} = 1$ we obtain $\bar{R_o} = 1.26$. After plugging the corresponding Helmholtz free-energy into Π_{int} and setting $\mu = 1$ as our reference value, we obtain the first results for both the internal pressure function (figure 5 (a)) and the phase diagrams (figure 5 (b)).

Figure 5 (a) shows the elastic stored energy within the material versus the stretch of the spherical wall, where the horizontal lines stand for total energy values (C). Let us now critically analyze it and describe whether it corresponds to oscillatory motion or not. It is a U-shaped curve, which means that for any and every C value (horizontal lines), there are two intersections with the function. This two intersections correspond to two particular moments at which both functions are equal, entailing as implied before that the total energy of the system is solely stored in the form of internal pressure or elastic stored energy. Moreover, this intersections happen to

occur at two clearly differentiated zones: on each side of the global minimum, where the function has different slope signs and not casually intersects the stretch at one. At this point, $\bar{r} = \bar{R}$, so the sphere is undeformed and all the energy needs to be kinetic unlike the other two intersection points just mentioned, where it needs to be potential (stored). Naturally, the evaluated function will be zero at the minimum. For $\lambda_i < 1$ and from the definition of the stretch, we have $\bar{r} < \bar{R}$, so the sphere is compressed and therefore the first intersection must correspond to the estate of maximum compression, where the velocity of oscillation is zero and the total energy equals the strain-energy function for Mooney-Rivlin's model. Similarly, when $\lambda_i > 1$, we have $\bar{r} > \bar{R}$, so the sphere is expanding. Therefore, the second intersection must correspond to the estate of maximum expansion, at rest, closing a loop motion that starts to be understandable as an oscillatory periodic motion.

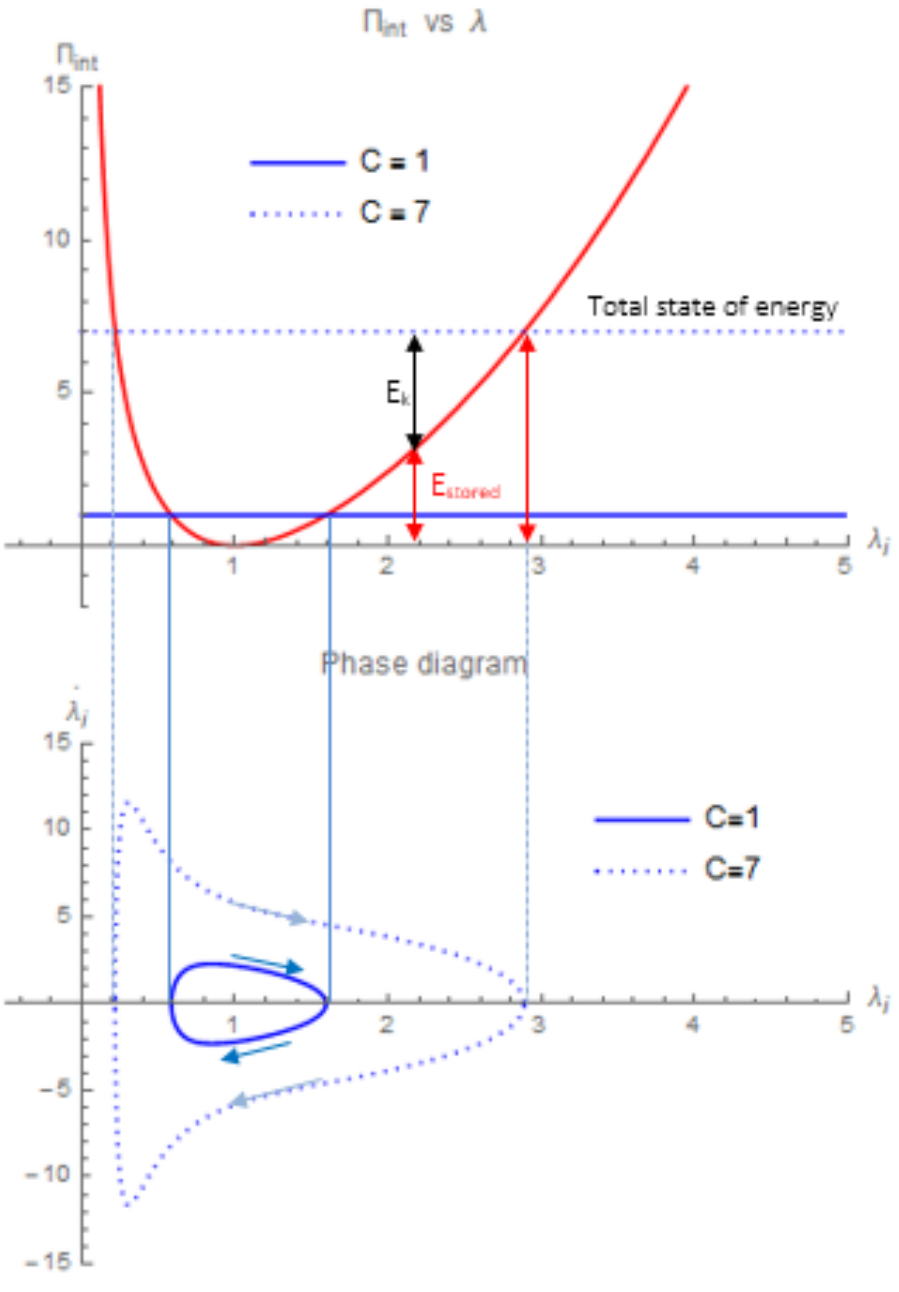

Figure 5. Free oscillations for Mooney-Rivlin materials with $\mu = 1$*. Two values for the initial conditions are studied: C = 1 and C = 7. (a) Strain-energy function versus stretch. (b) Phase diagram versus stretch.*

Regarding the range of the function, we have on the left-hand side of the graph that $\lim_{\lambda_i \to 0} \Pi_{int}(\lambda_i, \mu) = \infty$, and on the right-hand side $\lim_{\lambda_i \to \infty} \Pi_{int}(\lambda_i, \mu) = \infty$. Since there is no theoretical limit to the function on either side and it always behaves in the same concave manner, no matter which C value we have there will always be two intersections with the function and the same type of motion, as indicated above. Therefore we can say that in free-oscillations condition for Mooney-Rivlin materials there will always be oscillatory behavior. However if the energy level changes, for any stretch value, there will be different kinetic and potential energy distributions. See how, as indicated, for a total energy level of C = 7, at maximum stretch we find that the area below the function coincides with the total area, meaning that the total energy coincides with the stored energy. However, when there is an intermediate stretch, either in compressive or expansive motion, the area under the curve does not coincide with the total area or stored energy. Then, there must be some kinetic energy that complements the stored energy at that precise moment to reach the total amount of energy set for the system through the initial conditions (According to the conservation of energy principle).

Figure 5 (b) shows the first phase diagram of the document. It plots the wall's velocity versus its position (stretch). If the energy levels increase, the amplitude of the phase diagram increases as well, as indicated in figure 5 (b). Note also that both the stretch and the energy values need to be positive for the problem to make sense, so the negative quadrants are instinctively omitted. However, the phase diagram *does* include negative velocity values. When situated on the phase diagram's upper part, positive (expansive) velocity forces the sphere to have positive (outwards) stretch, so the sphere must undoubtedly move clockwise along the phase diagram.

Now let us point out that the phase diagram is a plot governed by linear velocity of the stretch against the stretch itself, forming a closed loop of infinite estates within which the sphere lies on, being unable to scape.

Observe as well, to completely understand figure 5, that the energy function is asymmetrical, because of the nature of strain-stretch plots. Due to this circumstance, the phase diagram is directly affected. Particularly, as C grows and the asymmetry takes action, modifying the slope of the function on each side at different rates, the shape of the phase diagram becomes altered. After the maximum compression estate (first intersection), as the sphere starts to expand, velocity brusquely shoots up to reach its maximum and then it diminishes as the sphere continues to expand. On the other side, when the oscillation is reaching the maximum compression estate again, it occurs just the opposite: velocity sharply drops to zero after reaching the same maximum absolute value.

Now, let us evaluate and comment the values obtained for different C's. As indicated above, for low values of C, the amplitude will be small, and for high, bigger. Specifically, for $\mathrm{C} = 1$ we find the first intersection at $\lambda_i = 0.586$ and the second at $\lambda_i = 1.594$ while for $\mathrm{C} = 7$ the obtained values are $\lambda_i = 0.219$ and $\lambda_i = 2.889$ respectively. If we recall the period calculation, from equation (25), we can also obtain the periods, T = 1.4512 for $\mathrm{C} = 1$ and T = 1.5084 for $\mathrm{C} = 7$. Indeed, a greater value for the initial conditions gives greater motion periods.

So far, we have only taken into account the relation of C with Π_{ext} and its influence on phase diagrams, but both strain-energy function and phase diagram also depend on the thickness parameter, set as one. However, it may not be one all the time, so it is interesting to analyze how it affects the function as well. To isolate the effect of the thickness, we will set C = 1 as the reference value this time.

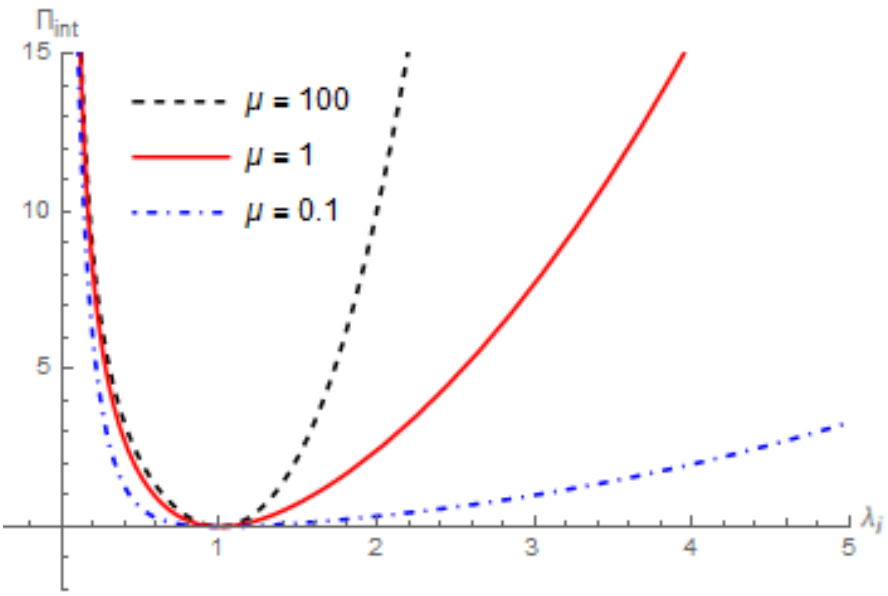

Figure 6. Thickness parameter influence on Mooney-Rivlin's constitutive model in free-oscillations.

There have been plotted extremely large ranges of μ. These values, 0.1 and 100, correspond to the following relations $1.032\ R_i = R_o$ and $4.657\ R_i = R_o$, acceptable values in a real consideration case. Independently of the spherical wall's thickness, the function presents a similar U-shaped behavior, but as μ decreases the storage capability for a certain stretch diminishes, and the curve flattens down. To counteract this energy loss (again, because of the conservation of energy principle), kinetic energy rises up to complete the total energy level. On the other hand, when the wall's thickness increases, there is more storage capability and the graph straightens up, seeking symmetrical behavior especially at low energy values. On the compression side, the fact that $\lim_{\lambda_i \to 0} \Pi_{int}(\lambda_i, \mu) = \infty$ and the necessity of $\Pi_{int} = 0$ for $\lambda = 1$ narrow the possibilities of noticeable changes in behavior when comparing different thickness values, and the graphs seem to be closer together.

Figure 7 evidences that for the same initial conditions, and assuming smaller thickness variations than showed in figure 6 (for the sake of clarity), the amplitude will increase if the thickness decreases. This occurs because the intersections that correspond to the maximum compression and expansion with the total energy are farther apart. Moreover, as C increases, this distance between intersections will increase for any thickness too, and the effect of a change in geometry will multiply for relatively high values of the initial energy.

Recall that still there must be an intersection at one for every graph, no matter what the thickness is, because it represents the value at which the sphere is undeformed with no stored energy (represented by Π_{int}), but at the same time there will be bigger velocities for lower thickness values to conserve total energy of the system,

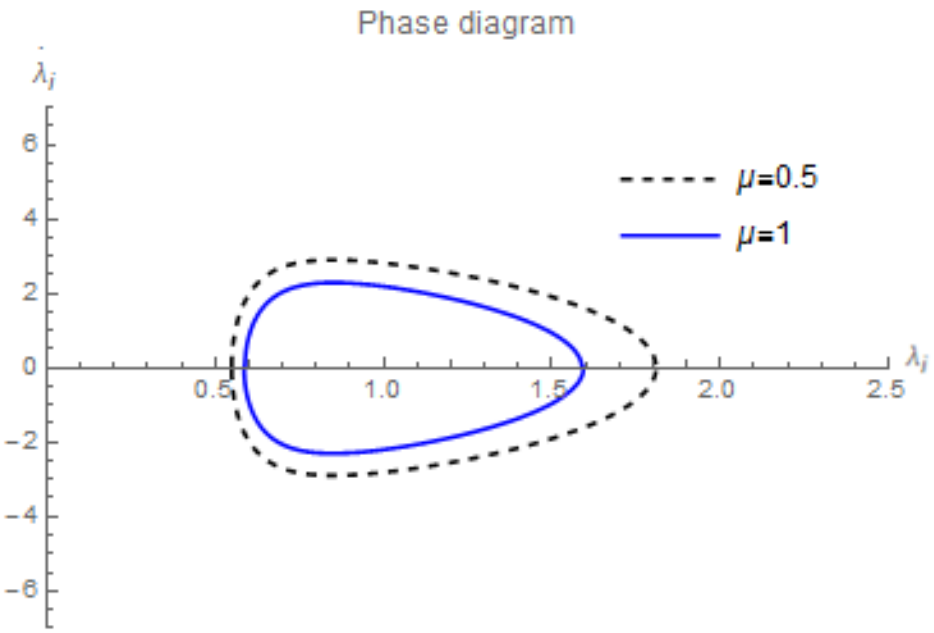

Figure 7. Thickness parameter influence on Mooney-Rivlin's phase diagram for a predefined total energy of C = 1.

4.2 Yeoh model

Recall that this constitutive model has, by definition, higher order invariants. It was already said that it captures the response of hyperelastic materials at large strains, so there are some differences expected regarding the previous subsection.

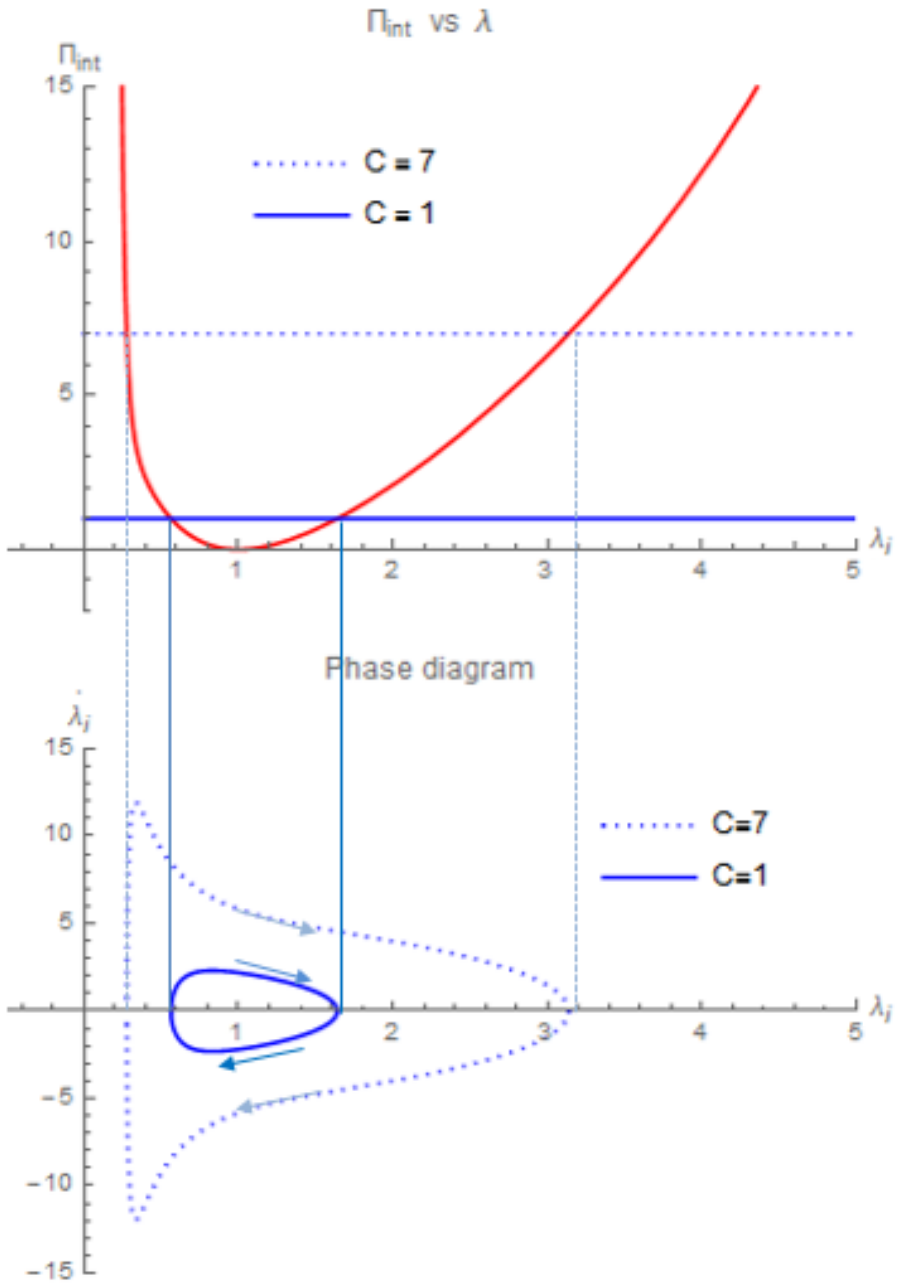

Figure 8. Free oscillations for Yeoh materials with $\mu = 1$*. Two values for the initial conditions are studied: C = 1 and C = 7. (a) Strain-energy function versus stretch. (b) Phase diagram versus stretch.*

Indeed, the curves are slightly different but the behavior and overall tendency is almost a duplicate. Note that Π_{int} maintains its shape regardless of the constitutive model and the thickness parameter. Since the form of the function still conserves the U-shaped configuration in all the existent range of C and λ, there will always be periodic motion as well. The intersection with the stretch naturally takes place at one too, but those intersections with the selected total energy values vary slightly. For C = 1, the values we find now for the maximum compression and maximum expansion are $\lambda_i = 0.564$ and $\lambda_i = 1.639$ respectively. The same values for C = 7 are instead $\lambda_i = 0.277$ and $\lambda_i = 3.137$. Again, if we take the period equation (23) and particularize it for this particular cases we obtain T = 1.5567 and T = 1.7016 for C = 1 and C = 7 respectively. In Yeoh materials, the phase diagram conforms a periodic, clockwise motion and the influence of C alters the velocity especially near the maximum compression estate in such a way that there is an extremely pronounced peak this time (see figure 8). Thickness influences the strain-energy function flattening the curve if the values are very low and straightening it up if the values are higher as mentioned before (see figure 9)

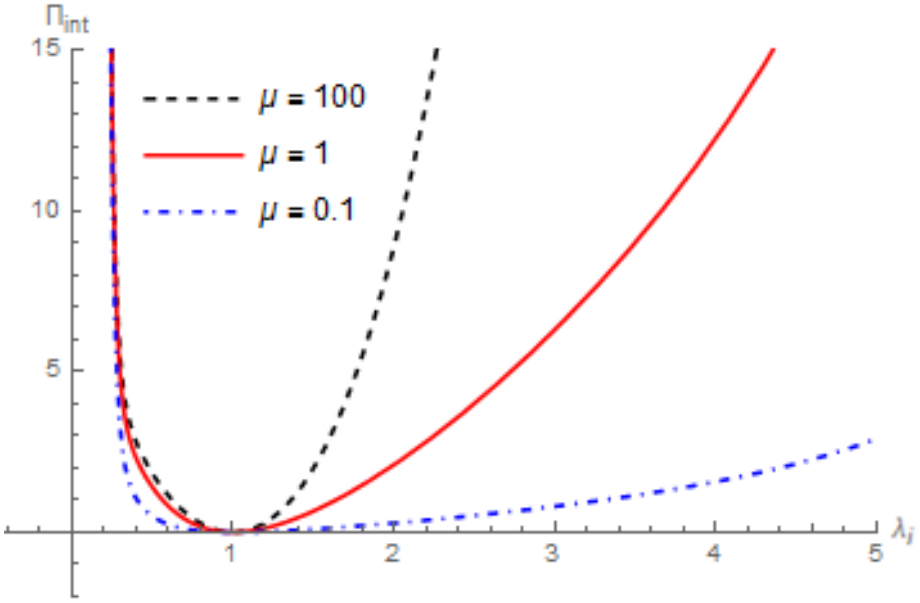

Figure 9. Thickness parameter influence on Yeoh's constitutive model in free oscillations

Moreover, lowering the thicknesses increases the amplitude, since the concave curve gets broader thus stretching the distance between intersections, as before. If another C value is set, the effect of the geometry is boosted. To demonstrate this effect we can observe figure 10 in which the fixed parameter is C = 1 and the variating parameter μ. Numerically, we find for $\mu = 1$, the maximum compression at $\lambda_i = 0.5637$ and the maximum expansion at $\lambda_i = 1.6393$. In the other case, $\mu = 0.5$, the same values are $\lambda_i = 0.5255$ and $\lambda_i = 1.8833$ respectively.

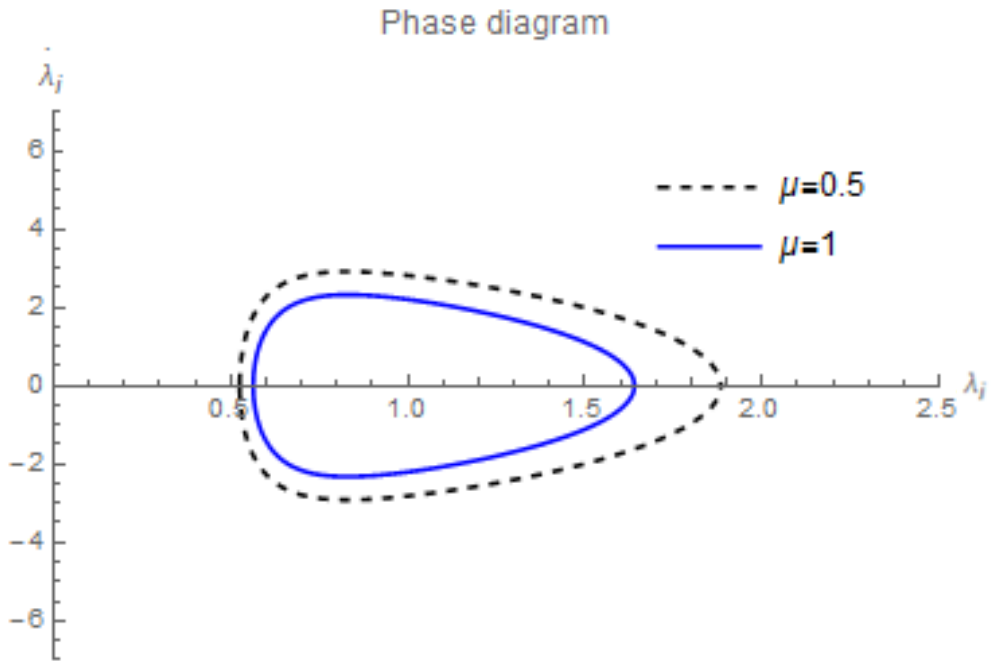

Figure 10. Thickness parameter influence on Yeoh's phase diagram for a predefined total energy of C = 1.

4.3 Conclusions

After analyzing both models in a free-oscillations situation, we can establish some conclusions. First, regarding internal energy:

- **There will always be oscillatory motion in both cases:** Both functions have an U-shaped concave form, meaning that there will always be two intersections with any total energy estate, which have already been said to correspond to the maximum compression and expansion estates.
- **Each function yields a different amplitude:** The functions have different slopes in most part of the path (especially further from the undeformed estate), so the distance between the intersections with C are different, causing different amplitudes (see numerical values in each subsection).
- **Infinite range of possible oscillations:** Neglecting failure (see section 6), both function share that $\lim_{\lambda_i \to 0} \Pi_{int}(\lambda_i, \mu) = \infty$ and $\lim_{\lambda_i \to \infty} \Pi_{int}(\lambda_i, \mu) = \infty$. Therefore, there is no theoretical limit on the amount of energy for which the system would not be able to oscillate.
- **Same thickness influence:** In both cases, we have that for lower values of the selected reference thickness, the system absorbs less energy, in favor of the kinetic energy (as explained because of the energy conservation principle). This graphically causes the function to flatten down. On the contrary, higher thicknesses values allow the sphere to retain more energy, straightening up the function in both cases.
- **Higher C values amplify the thickness influence**: As the total energy increases, each side of the function goes in a different direction tending to infinity. The branches of the function constantly move away from each other. Then, we can say that an increase in C pulls the intersections away, thus multiplying the effect of thickness and increasing the amplitude.

Second, regarding the phase diagrams. We have already said that there will always be oscillatory motion, meaning that the phase diagrams will always conform a closed loop in the phase plane. However, there are some other results worth remarking:

- **Almost Identical maximum velocities:** For the case C = 1, Mooney-Rivlin materials reach a maximum velocity of 2.304 at $\lambda = 0.850$ while Yeoh materials reach 2.320 at $\lambda = 0.831$, barely higher. Moreover, for a much greater energy value (seven times larger), the maximum velocities are still alike: 11.595 at $\lambda = 0.305$ for Mooney-Rivlin constitutive model and 11.934 at $\lambda = 0.335$ for Yeoh's.
- **Yeoh materials have greater oscillation periods when dealing with low energy values:** As anticipated previously, Yeoh materials will have slightly greater periods. Recall that the period formula is the numerical integration between the intersection points of the inverse of the velocity. Then, Yeoh's bigger amplitudes (broader integration limits) and almost identical velocities leads to Yeoh material's greater periods, as we can see in figure 11. Moreover, the temporal behavior as the total energy values increase initially follows

the same tendency. They both grow logarithmically until a certain point, C = 25 in Mooney-Rivlin materials and C = 11 in Yeoh materials, where this demeanor is reversed. Note that Yeoh material's curve (said to capture the response at large strains, implied by greater C values) drastically drops while Mooney-Rivlin's trajectory decreases smoothly. Around C = 28, the period values intersect and Mooney-Rivlin constitutive model displays greater values for the same amount of total energy.

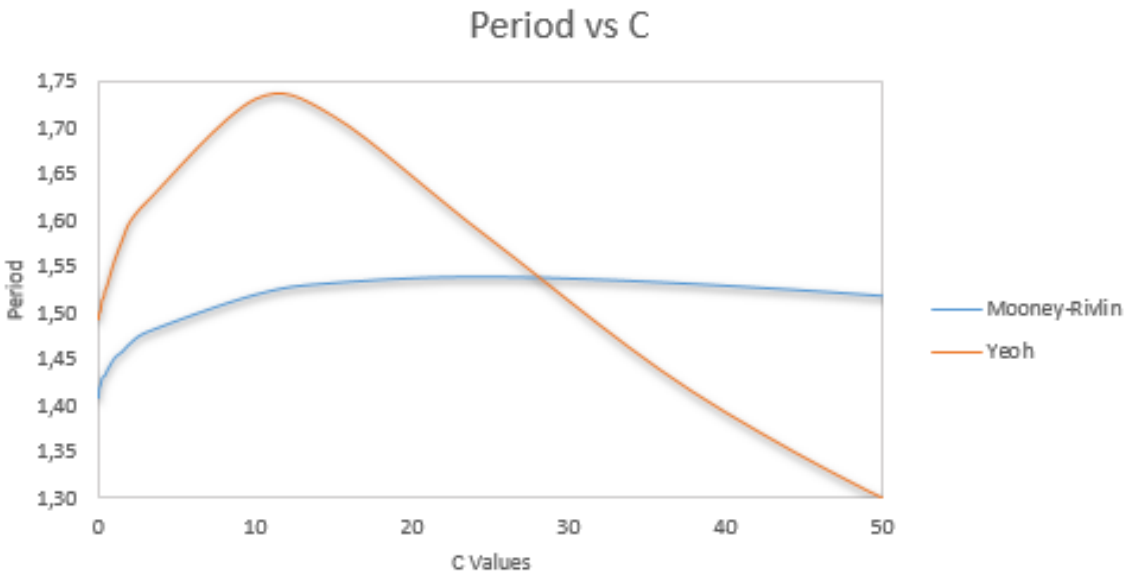

Figure 11. Total energy influence on period. Comparison between Mooney-Rivlin and Yeoh materials within the range C = (0,60).

Chapter 5: Forced oscillations

Now, we investigate the influence of applied constant pressures on the spherical shell, this is forced oscillations. In order to isolate the effect caused by them, we will set a initial estate of rest as our initial condition, where the stretch equals the unity and therefore its derivative (the radial velocity) zero. Thus, the initial energy becomes null, yielding the following phase diagram

$$\dot{\lambda_\iota} = \sqrt{\frac{-\Pi_{ext} - \Pi_{int}}{\lambda_i{}^2\left(1 - \frac{\lambda_i}{\sqrt[3]{\mu + \lambda_i{}^3}}\right)}} \tag{35}$$

where now the roots of the function are not only not dependent on C but more important, they now depend on the external pressure term, which is a non-linear term. This causes the numerator to behave differently and modifies the number of existing roots, which is the principal difference with free oscillations. Along with roots variation comes phase diagram variation and therefore we will no longer have the oscillatory motion for all situations when dealing with forced oscillations that we saw in free oscillations. Let us seek the outcome in this conditions.

5.1 Mooney-Rivlin model

To analyze Mooney-Rivlin's consitutive sensitivity of the oscillatory behavior depending on different pressures values, we will scan the internal energy and phase diagram demeanors in the whole significative range of pressure values and set $\mu = 1$ to isolate the pressure effect. Then, the most representative value for each peculiar range (where the behavior is conserved) will be plotted and described. For descriptive purposes and clarity, there will be used three figures to describe the behavior of these materials depending on the selected pressure values.

First range of pressures

- $0 < \Delta\bar{P} < 0.1657$. One round representative value of the range will be $\Delta\bar{P} = 0.15$. As we can notice in figure 12 (a), the internal energy has at the beginning two intersections. The first one corresponds to the rest initial estate (boundary condition in forced oscillations), and the second one closes the loop for an oscillatory motion.
- $\Delta\bar{P} = 0.1657$. This has been found to be a critical pressure value. There is a change in the curve that eventually makes it tangent to the axis from below (zero velocity), provoking a third intersection point. At that exact point, the phase diagram would include an open curve (non-oscillatory motion) apart from the closed loop we would still find on $\bar{r} = \bar{R}$. The open curve represents an instable behavior that implies not oscillatory motion because velocity and stretch increase up to infinity with infinite expansion as well. However, it has been previously stated that the initial condition in forced oscillations is that the stretch must be one, therefore any closed or open phase diagram loop that does not go through that point is not valid.

- $0.1657 < \Delta\bar{P} < 0.25$. Right after reaching the critical value, the function acquires a different shape which now causes four intersections, meaning two separated closed loops that define oscillatory motion. A value that represents this motion range is $\Delta\bar{P} = 0.17$. Again, this closed loop is not valid for the same reason as before: it is located out of the boundary conditions. Thus, we can establish that this critical pressure has no theoretical valid influence on the model.

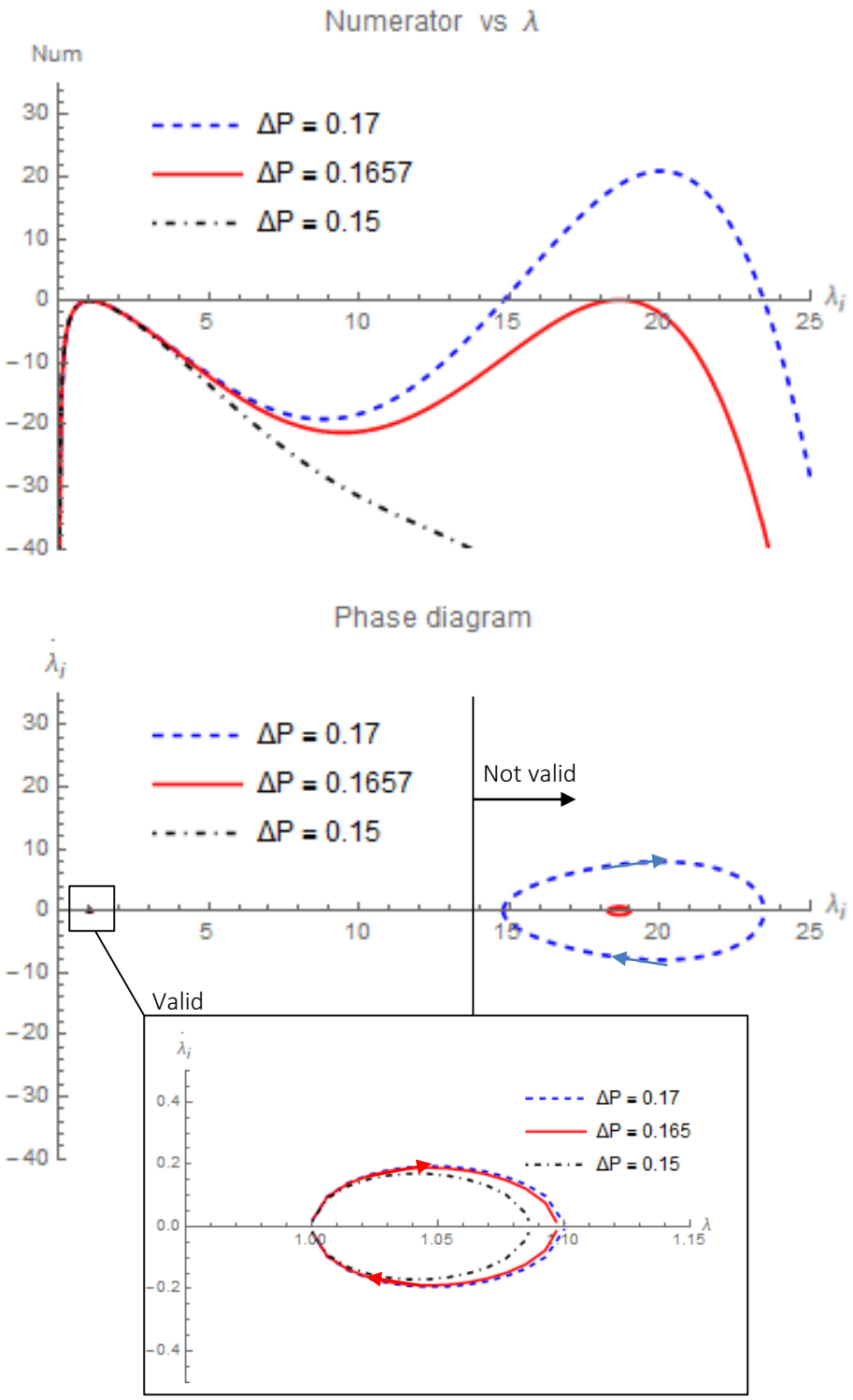

Figure 12. Forced oscillations for Mooney-Rivlin materials with $\mu = 1$. First critical pressure value. (a) Numerator function versus stretch. (b) Phase diagram versus stretch. (c) Zoom on phase diagram for the valid loop in the phase plane, according to the initial conditions.

Note that the amplitude of the valid oscillations for such low pressure values are extremely small compared to those obtained in free oscillations. As the pressure keeps increasing, there is a moment from which the last intersection no longer appears, because $\lim_{\lambda_i \to \infty} \Pi_{int}(\lambda_i, \mu) = \infty$. It only implies what we have stated earlier for $\Delta\bar{P} = 0.1657$: there would be an open curve again beyond the first closed loop that delimits the valid oscillatory motion. Nonetheless, the whole curve continues shifting up and a second scanning is necessary.

Second range of pressures

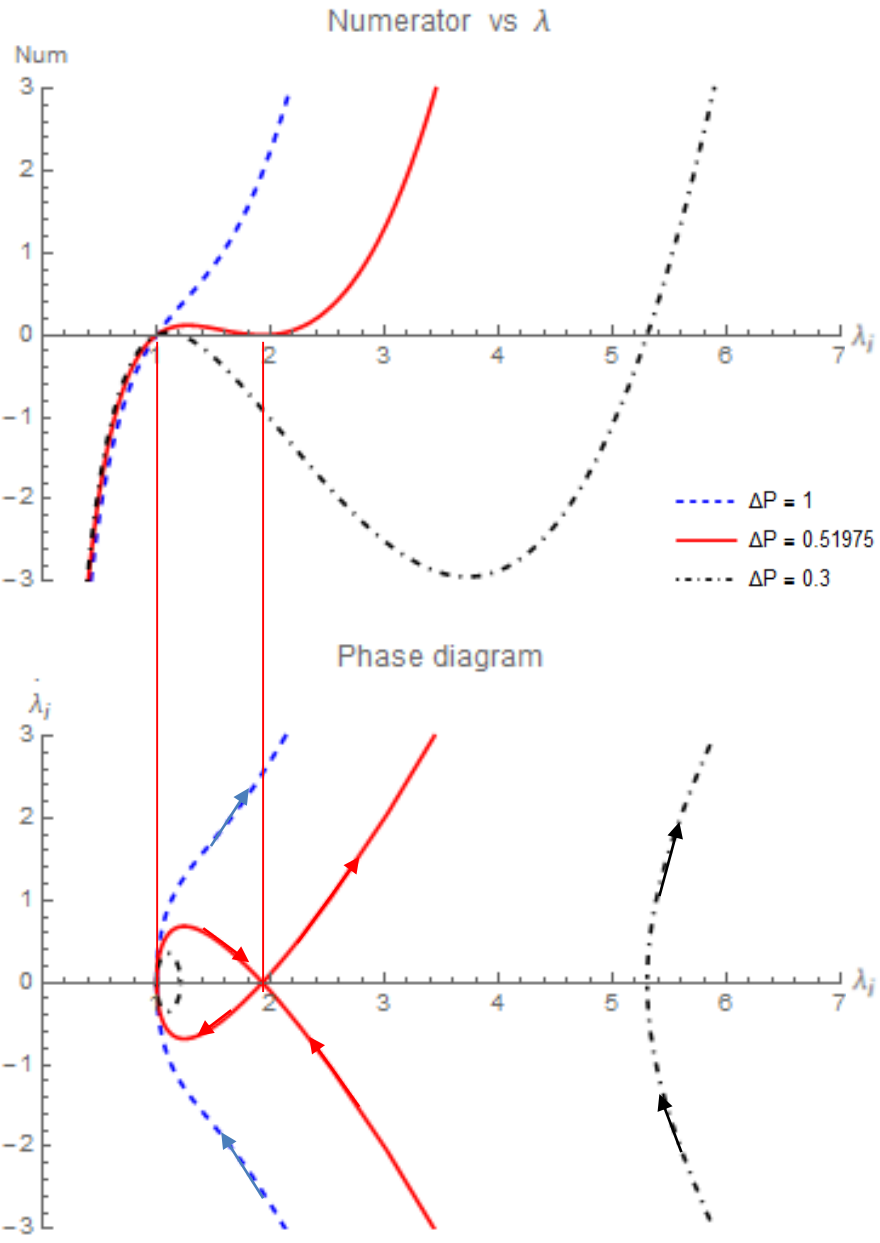

Figure 13. Forced oscillations for Mooney-Rivlin materials with $\mu = 1$. Second critical pressure value. (a) Numerator function versus stretch. (b) Phase diagram versus stretch. Critical relation between numerator and phase diagram indicated.

Again, there have been some representative values selected for each range with different outcomes.

- $\Delta\bar{P} = 0.3$. Here $\Delta\bar{P} < \Delta\bar{P}_{critical}$. The expression $-\Pi_{ext} - \Pi_{int}$ has three real roots. The first one accounts for the initial condition. The second one is located at $\lambda = 1.211$ and closes the loop. The third one corresponds to the open curve and it is located at $\lambda = 5.303$.
- $\Delta\bar{P} = 0.51975$. Here $\Delta\bar{P} = \Delta\bar{P}_{critical}$. This is the limit of the oscillatory behavior. The second intersection takes place at $\lambda = 1.934$, after which the sphere could either oscillate and initiate its compression or keep expanding up to infinity with a monotonically growing velocity as well, in a non-oscillatory motion. This is because $\lambda = 1.934$ is a point of inestability and theoretically there exist two solutions, being the outcome assuredly unknown.
- $\Delta\bar{P} = 1$. Here $\Delta\bar{P} > \Delta\bar{P}_{critical}$. In any case we have this condition, the roots (only one per each pressure and C values) define open curves in the phase plane for which oscillatory motion can not exist. Moreover, the root will always be at $\lambda = 1$, which recall is the initial condition estate.

While the first critical case was discarded as relevant because it only affected the area outside our boundary conditions, this second critical case tells us just the opposite. When the function (that already has three intersections) shifts up, it reaches a point where the number of real roots changes from three to only two, when the line is superiorly tangent to the axis: that is the second instability point, which is now relevant because it implies a valid change in behavior. Immediately after, the function straightens up and leaves behind its path only one intersection, so the phase diagram will be an open curve whose extremes will tend to infinity (and so will radial velocity).

Third range of pressures

We have only examined positive pressure values so far. It was implied that $\Delta\bar{P} = \bar{P}_i - \bar{P}_o$ and $\bar{P}_i > \bar{P}_o$ because the initial undeformed estate corresponds with the maximum compression of the system, and then it expands. However, it can occur that the outer pressure be greater than the inner pressure, leading to negative $\Delta\bar{P}$ values (see figure 14). In such case, we will have, independently of the pressure value, two roots in $-\Pi_{ext} - \Pi_{int}$. Therefore, for negative pressure values there will always be periodic motion with an estate of maximum expansion at $\lambda = 1$ and minimum compression at $\lambda < 1$ depending on the chosen pressure.

Particularly, with $\Delta\bar{P} = -7$ the maximum compression estate corresponds to $\lambda = 0.2961$ and with $\Delta\bar{P} = -3$ to $\lambda = 0.4814$. Note that as the (absolute value) pressure increases, the closed loop starts to behave in the same manner it did in free oscillations, reaching a peak of maximum velocity after the maximum compression to then decrease the velocity progressively as the sphere stretches. As for the thickness influence, we have observed the same effect as before: an increase in the wall's thickness decreases the amplitude.

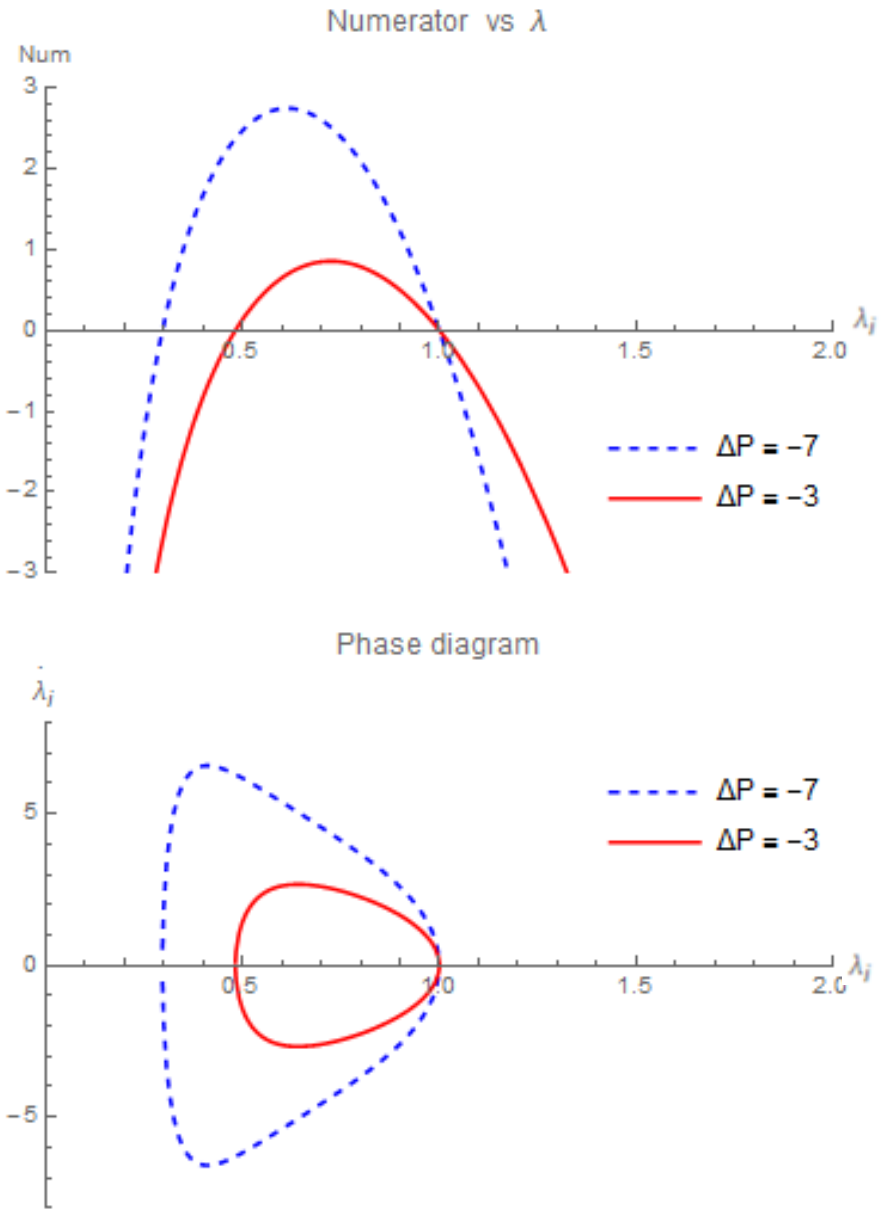

Figure 14. Forced oscillations for Mooney-Rivlin materials with $\mu = 1$ *and negative pressures. Two cases studied,* $\Delta\bar{P} = -3$ *and* $\Delta\bar{P} = -7$*. (a) Numerator function versus stretch. (b) Phase diagram versus stretch.*

5.2 Yeoh

In this subsection, we distinguish three different behaviors depending on the examined range. Let us investigate what happens on them for a better understanding. This time only one figure will be enough to scan every distinctive range.

- $0 < \Delta\bar{P} < 0.45213$. The representative chosen value is $\Delta\bar{P} = 0.3$. Below Yeoh's critical pressure value, there are four roots in the phase diagram equation. The first two correspond to a closed loop in the phase plane, defining again one valid oscillatory motion. The other two define a closed loop in the phase diagram but again, out of the valid range.
- $\Delta\bar{P} = \Delta\bar{P}_{critical} = 0.45213$. The function reaches a critical pressure for which there are three roots that conform two contiguous oscillatory motions. This is another instability point, $\lambda = 1.8591$. Here there exist two possible solutions, either a concatenation of two contiguous oscillatory motions or a regular oscillatory motion with maximum expansion at the critical point. In the case of two contiguous oscillations, the maximum expansion of the first one (again, $\lambda = 1.934$) corresponds to the minimum compression of the second one.
- $\Delta\bar{P} > 0.45213$. The selected value will be $\Delta\bar{P} = 0.48$. After $\Delta\bar{P} > \Delta\bar{P}_{critical}$, the valid and not valid oscillations merge together and form only one big oscillatory motion with only two real roots that start at $\lambda = 1$. Therefore, the amplitude of the oscillation expands from a maximum stretch of $\lambda = 1.8591$ before the critical pressure to a maximum of $\lambda = 8.4855$, almost five times greater. Moreover, not only the amplitude boosts above the critical value, but the velocity also boosts, reaching its maximum near the maximum expansion estate for the first time in the whole investigation. Since the behavior stays the same in time as pressure increases, there will always be oscillatory motion in Yeoh materials for positive pressure values in forced oscillations too.

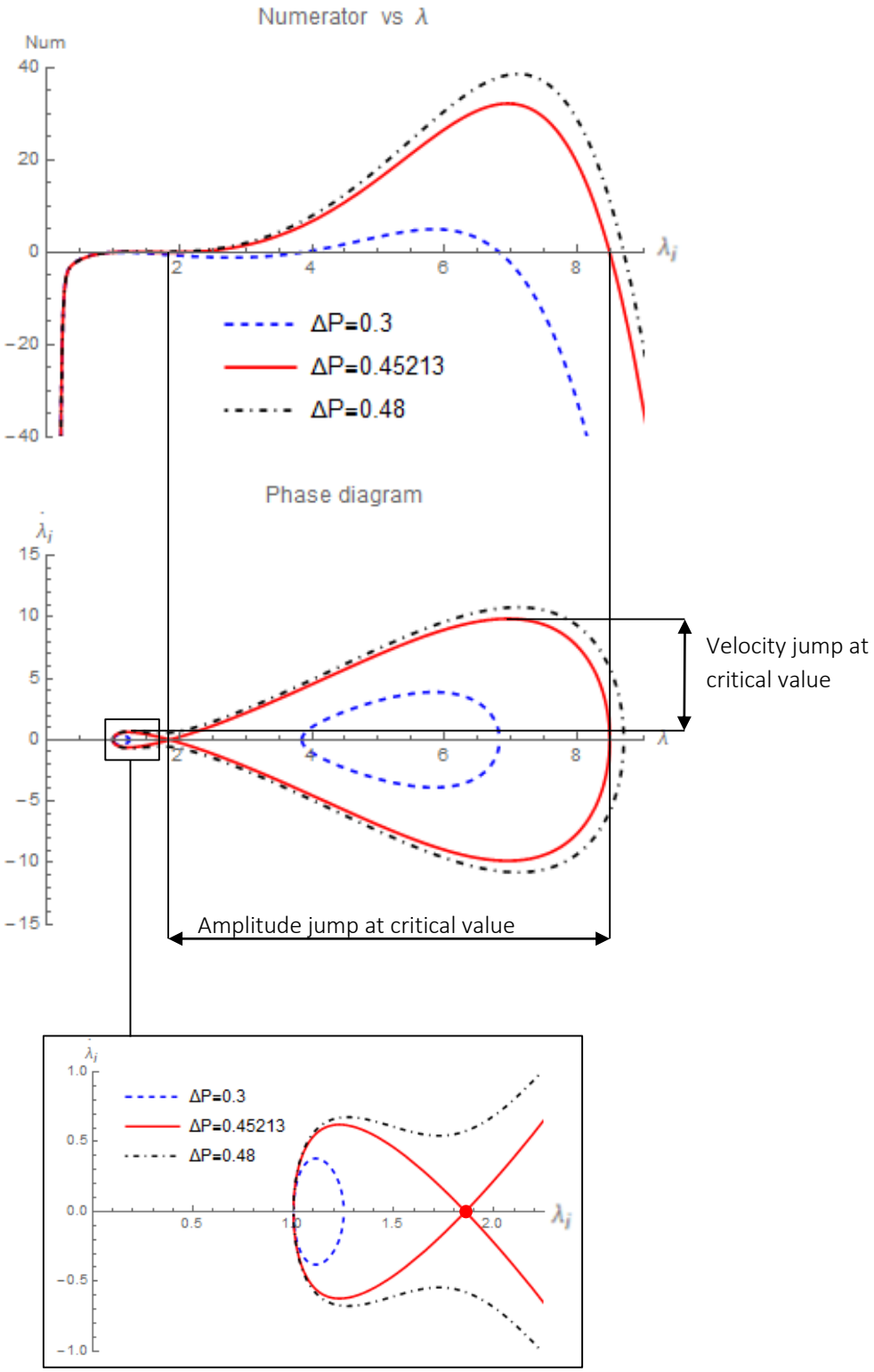

Figure 15. Forced oscillations for Yeoh materials with $\mu = 1$.. *Three cases studied,* $\Delta\bar{P} = 0.3$, $\Delta\bar{P} = 0.51975$ *and* $\Delta\bar{P} = -0.48$. *(a) Numerator function versus stretch. (b) Phase diagram versus stretch.*

Regarding negative pressures, we again study the same two different values as in Mooney-Rivlin materials to facilitate comparison afterwards. The result is the following: Same behavior, with two roots in all the functions range. For $\Delta\bar{P} = -7$, we find the maximum compression at $\lambda = 0.3059$, while for $\Delta\bar{P} = -3$, it is at $\lambda = 0.4473$ (see figure 16). Maximum velocity is reached near maximum compression too, and then it decreases in time as the sphere expands.

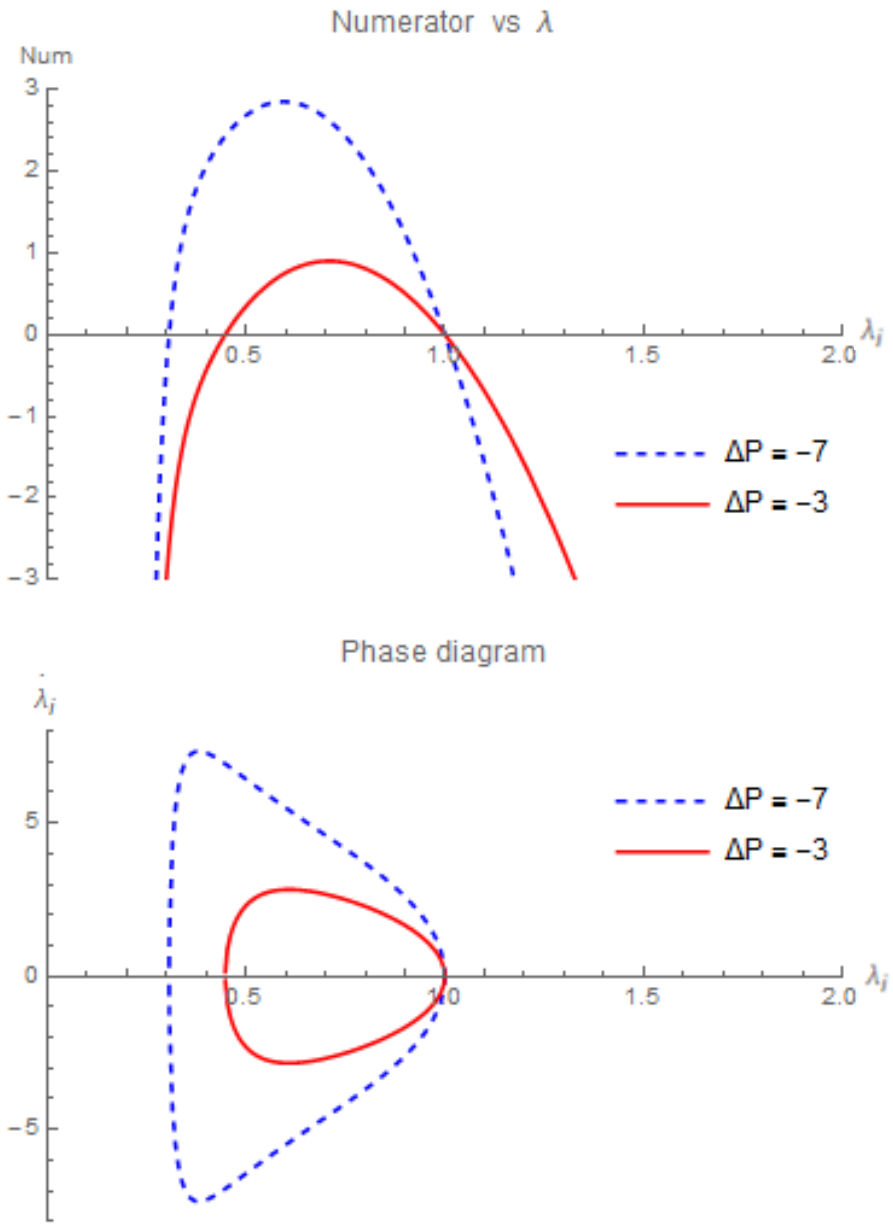

Figure 16. Forced oscillations for Yeoh materials with $\mu = 1$ *and negative pressures. Two cases studied,* $\Delta\bar{P} = -3$ *and* $\Delta\bar{P} = -7$*. (a) Numerator function versus stretch. (b) Phase diagram versus stretch*

5.3 Conclusions

Forced oscillations yield very different results depending on the selected constitutive model. Regarding positive pressure values:

- **Critical pressure values influence:** Mooney-Rivlin materials have two critical cases while Yeoh materials just one. The first critical case in Mooney-Rivlin materials arises for relatively low pressure values and gives no useful information because it is out of the coherent range of motion, defined by the initial conditions. The second one (located at $\lambda = 0.51975$) defines the limit of oscillatory motion. However, for Yeoh materials the critical point is located at $\lambda = 0.45213$ (earlier than on Mooney-Rivlin constitutive model). At that point occurs just the opposite. The oscillatory behavior suffers a great jump in amplitude and velocity, almost five times bigger (4.7), maintaining an oscillatory status in all the existing range of pressure. Therefore, Yeoh materials will oscillate for any theoretical pressure condition (recall failure limit due to maximum stress or velocity is not analyzed in this first approach investigation due to complexity).

- **Yeoh's velocity alteration:** While in previous sections the maximum velocity was always situated near the maximum compression estate or halfway through the oscillation, in forced oscillations and after reaching the critical point, this tendency is reversed. For values immediately bigger than the critical pressure value, there is a local maximum near the maximum compression estate, then a local minimum around $\lambda = 0.45213$, precisely the stretch at which we had the second root for the critical pressure, and then the global maximum near the maximum expansion. However, the local minimum disappears with time if we apply enough pressure, being its location near the maximum compression (as in free oscillations). Regarding Mooney-Rivlin materials phase diagram's velocity, there is no oscillation above the second critical pressure and thus velocity would tend to infinity along with the stretch.

As for the negative pressures:

- **Both models always have oscillatory motion:** No matter which pressure value we define, there will always be closed loops in the $(\dot{\lambda}, \lambda)$ plane.

- **Both models yield almost identical periods for the whole negative pressure range:** Since both models present oscillatory behavior in the whole negative pressures range, it is interesting to compare the period. In the analyzed cases, we obtain for $\Delta\bar{P} = -3$ a period T = 0.6356 for Mooney Rivlin materials and T = 0.6450 for Yeoh materials. In the case of $\Delta\bar{P} = -7$, Mooney-Rivlin materials achieve T = 0.4178 and Yeoh materials T = 0.4015. Indeed, we can see figure 16 that for a very broad range of pressures (from -1 to -25) there are almost identical periods.

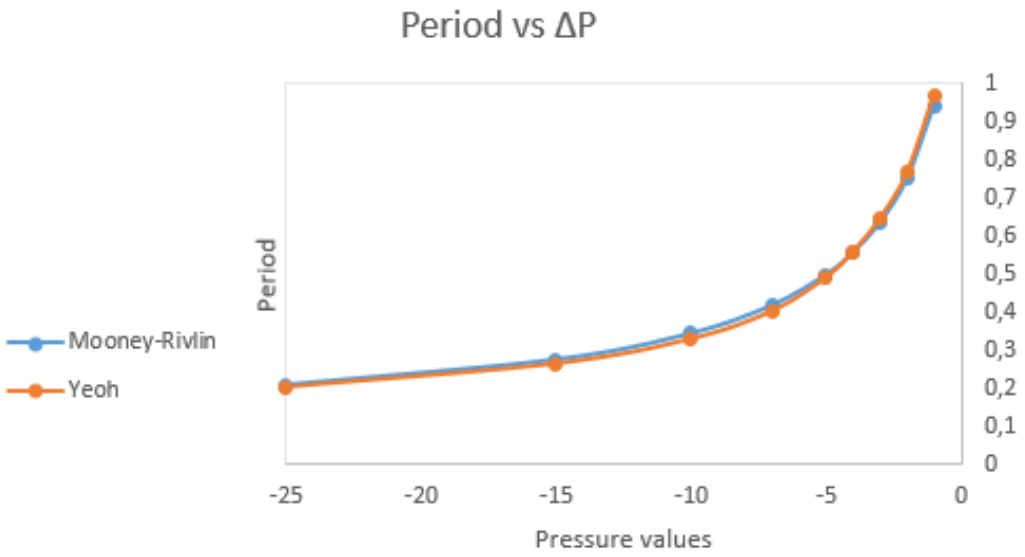

Figure 17. Pressure influence on period. Comparison between Mooney-Rivlin and Yeoh materials for negative pressure values within the range $\Delta \boldsymbol{P}$ = (-25,-1).

Chapter 6: Final conclusions and overview

In this section we will chronologically

1. Determine whether the objectives have been successfully accomplished after the investigation.
2. Analyze the obtained results.
3. Draw admissible conclusions, and
4. Consider those aspects that could be further investigated to improve the work done.

6.1 Objectives

In section 1 (Introduction and importance of the work) we defined two type of objectives. The first were denominated as intermediate objectives, necessary to understand the context in which the problem is placed and crucial in order to start developing the investigation. Here there were included issues such as understanding hyperelastic materials, developing the corresponding mathematical operations or being able to use a program powerful enough to achieve conclusive results. In the end, an extensive study on hyperelastic material oscillations has been auspiciously performed and in view of the results, we can cheerfully confirm that each intermediate objective has been successfully completed.

Moreover, we have acknowledged the importance and relevance of engineering on a different ambit (a physiological scope exactly) and have been able to apply theoretical, learned knowledge, which is a demonstration of auto determination and initiative.

6.2 Results

Regarding the ultimate objectives, free and forced conditions have been simulated successfully with convincing outcomes. These situations have been analyzed independently, but now their effects will be compared along with the constitutive sensitivity exposed by the different material models. Here are the conclusions:

- **An increase in the initial energy constant (free oscillations' analysis) causes continuous smooth evolution of the phase diagrams while an increase in pressure (forced oscillations) causes phase diagram's dramatic alterations.**

  In free oscillations we isolated the effect of the initial energy for each material model. An increase in the initial energy implies:

  I. Greater amplitudes (always) and periods (up to a certain point of relatively high energy). The physical reason behind it is that the extra energy is introduced in the system only kinetically. Therefore, at any estate of maximum expansion

corresponds certain amount of elastic stored energy which equals the total energy, but with an increase of energy will only add kinetic energy, this is motion, prolonging the oscillation in space and time.

II. A shift in maximum velocity's location towards the beginning of the expansion and a different velocity time distribution. As indicated in section 4, there is a sharp peak of velocity near the maximum compression estate. Then, it drops smoothly until the sphere reaches the maximum expansion estate. When we have negative velocities (the sphere compresses) the energy distribution behaves equally acquiring a symmetrical shape.

In forced oscillations we isolated the effect of applied constant pressure, yielding the following results:

I. Mooney-Rivlin materials reach a critical positive pressure value ($\Delta\overline{P} = 0.51975$) that defines the limit of the oscillatory behavior. When the sphere has this critical pressure, there is an instability point ($\lambda = 1.934$) at which there exist two possible outcomes: either oscillation or infinite expansion. Above it, there will always be infinite expansion.

II. Yeoh materials reach a critical positive pressure value ($\Delta\overline{P} = 0.45213$) that causes the oscillations to boost almost five times in amplitude and maximum velocity for the whole range of pressures. The instability point ($\lambda = 1.8591$) delimits whether the sphere oscillates with very low or very high amplitude and velocity values.

III. Mooney-Rivlin materials reach maximum velocity near the maximum compression estate, as they did in free oscillations. However, when Yeoh materials overcome the critical point, two contiguous oscillations merge together, being the maximum velocity located near the maximum expansion estate for the first time during the whole investigation.

Because an initial condition of rest was set, the oscillations must start at $\lambda = 1$. Nonetheless, the sphere can either expand or compress, depending on the sign of the pressure value. In negative pressure values investigations we find:

IV. Both materials behave identically. There is always oscillatory motion and the maximum velocity is located towards the maximum compression estate. Again, it decreases smoothly as the sphere expands.

- Thickness affects both constitutive models equally.

Independently of the type of oscillation, an increase in the sphere's wall provides more energy storage capability. Then, due to the energy conservation principle, kinetic energy will be reduced shortening the amplitude of the oscillation and lowering the velocity throughout the whole period. Moreover, in forced oscillations this store capability gain not only reduces the kinetic energy, but it also delays the critical pressure value. The shell is able to store more energy so it would be equivalent to having less pressure. In figure (13) we can see a plot of Mooney-Rivlin and Yeoh materials' phase diagrams ((a) and (b) respectively) at their critical pressure for different thicknesses. Note that an increase in the thickness will delay the critical pressure value, so there would still be oscillatory motion at the critical pressure value (for the reference thickness).

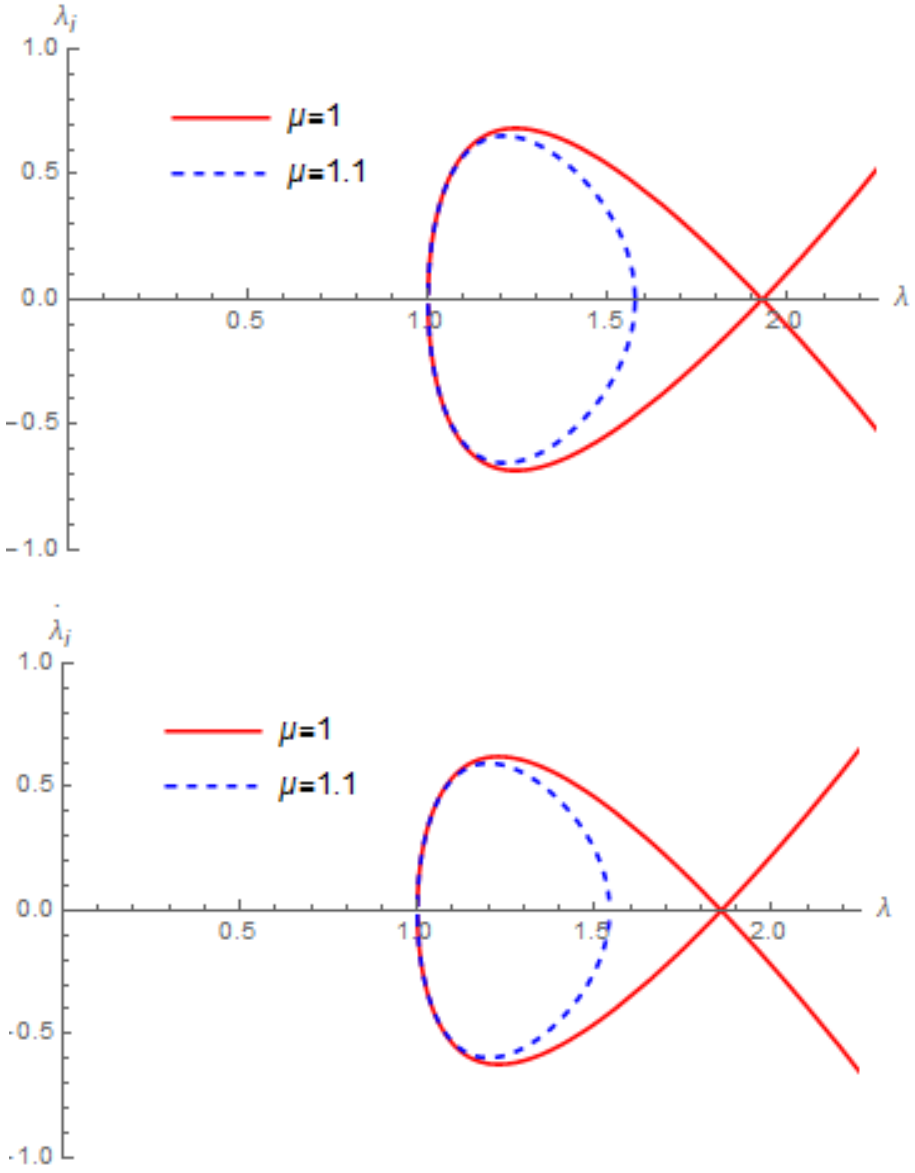

Figure 187. Thickness influence on critical pressure values. (a) Mooney-Rivlin materials, $\Delta\bar{P} = \mathbf{0.51975}$. *(b) Yeoh materials,* $\Delta\bar{P} = \mathbf{0.45213}$.

- **In free oscillations, Yeoh materials yield greater periods. In forced oscillations (with negative pressures) the periods are the same.**

  It was already mentioned in subsection 4.3 that Yeoh materials have greater periods regarding free oscillations. The period in both cases follows a logarithmic growing evolution until a certain point where it starts to decrease (for relatively high energy values). In forced oscillations the comparison only makes sense with negative pressure values, where the periods are almost identical. When there are positive pressure values the models will not behave alike so there is no point in comparing them.

6.3 Conclusions

In the end, it has been developed a two constitutive models systematic comparison, from which we need to do some closure. From the theoretical expression of the Helmholtz free-energy we already know that Yeoh materials capture the response to large strains due to higher order I_1. Regarding free oscillations, this datum translates into greater amplitudes and periods. As the initial energy increases, the models (that behave mostly identical) start to diverge, but at a very slow rate. Thickness effect does not affect this choice because it basically implies the same variations.

However, forced oscillations are a different case. Depending on the model chosen, there is a critical pressure value above which there is a change in behavior. In Mooney-Rivlin materials we have seen that beyond that point there is infinite expansion, causing rupture of the sphere independently of the failure criteria used. Meanwhile, Yeoh materials boost their oscillations, which will increase amplitude and velocity as pressure increases, but always maintaining the oscillatory behavior. Therefore, Mooney-Rivlin materials can be considered to be more conservative, thus giving a safe margin of error.

Another conclusion we extract from the investigation is that it is necessary a calibration under dynamic estates to determine the constitutive models. Both models are used indistinctly in hyperelasticity and were calibrated statically. Moreover, in free oscillations it did not implied dramatic consequences, but when it came down to forced oscillations and pressure was applied the models showed completely different behaviors.

6.4 Improvements

In this document there has been developed a first approach for a problem on non-linear radial oscillations of hyperelastic spherical structures. However, there is still work ahead and further investigations that can be done. There have been made some assumptions which simplify the problem, but in order to approach real life conditions more accurately. Here are some notions to be implemented in further investigations:

- **Considering compressible materials:** In real life cases, there are no incompressible materials. Some are said to be incompressible enough for relatively low stresses, over certain distances or time scales. However, under powerful enough forces they all are compressible. Therefore it would be interesting to evaluate the results for compressible materials.
- **Considering failure criteria:** In free oscillations, there is no theoretical limit to the oscillations for any constitutive model. However, no material is able to absorb infinite energy without bursting, so there are some failure criteria to be considered, due to wall's strength, or maximum stretch or velocity. In forced oscillations, Mooney-Rivlin materials will stop oscillating at the instability point, but there could be rupture before reaching that point. Naturally, for Yeoh materials occurs the same. They will not oscillate forever in forced oscillations as predicted so, again, there needs to be a failure criterion.
- **Considering unsymmetrical deformation and anisotropy:** Due to the physiological framework, the structure is not a perfect sphere. It bulges on the artery's weakest spot, thus lying on it. This can cause uneven inflation and anisotropy (uneven material properties distribution) within the sphere, or the aneurysm can also be fusiform, meaning there is no spherical shape. Although it is the most complex issue to analyze in detail, it could be done using finite element method help on computer programs.

Appendix A: Material constants and other parameters

- **Dimensionless time variable deduction**: The dimensionless time variable deduction comes after the introduction of all the other dimensionless parameters. When they are introduced in equation (3), it turns into

$$\frac{\partial(\bar{\sigma}_r C_{10})}{\partial(\bar{r}R_i)} + 2\,\frac{(\bar{\sigma}_r - \bar{\sigma}_\theta)\,C_{10}}{\bar{r}R_i} = \rho\frac{\partial^2(\bar{r}R_i)}{\partial(\tau\, t_0)^2}$$

which can be rearranged as

$$\frac{\partial\bar{\sigma}_r}{\partial\bar{r}} + 2\,\frac{(\bar{\sigma}_r - \bar{\sigma}_\theta)}{\bar{r}} = \frac{\partial^2\bar{r}}{\partial\tau^2 {t_0}^2}\,\boldsymbol{\rho}\,\frac{\boldsymbol{R_i^2}}{\boldsymbol{C_{10}}}$$

so we can set t_0 equal to

$$t_0 = R_i\sqrt{\frac{\rho}{C_{10}}}$$

and ${t_0}^2$ will cancel the last fraction out so that the final dimensionless equation becomes $\frac{\partial\bar{\sigma}_r}{\partial\bar{r}} + 2\,\frac{(\bar{\sigma}_r - \bar{\sigma}_\theta)}{\bar{r}} = \ddot{\bar{r}}$.

- **Material constants**

Mooney-Rivlin material constants (Pa)	
α	210 587.307
β	1 504.76719

Yeoh material constants (Pa)	
C_1	190 592.559
C_2	-1 634.89996
C_3	41.3399927

- Dimensionless constant for stresses: for simplicity we will set

Dimensionless constant	
C_{10}	α

- Terms in Yeoh's elastic stored energy

  - $A = \frac{\left(\left(\frac{\lambda^3+\mu}{1+\mu}\right)^{\frac{1}{3}}\cdot\left(1-2\lambda^3-\mu\cdot\lambda\right)+\lambda\cdot\left(2\lambda^3+\mu-1\right)\right)}{\lambda*\left(\frac{\lambda^3+\mu}{1+\mu}\right)^{\frac{1}{3}}}$

  - $B = \frac{1}{5\lambda^5}+\frac{4}{5\lambda^2}-\frac{6}{\lambda}-8\lambda+12\lambda^2+4\lambda^4+3\mu-\frac{1+\mu}{5\left(\frac{\lambda^3+\mu}{1+\mu}\right)^{\frac{5}{3}}.}-\frac{4(1+\mu)}{5\left(\frac{\lambda^3+\mu}{1+\mu}\right)^{\frac{2}{3}}.}+\frac{6(1+\mu)}{\left(\frac{\lambda^3+\mu}{1+\mu}\right)^{\frac{1}{3}}.}+8(1+\mu)\left(\frac{\lambda^3+\mu}{1+\mu}\right)^{\frac{1}{3}}\cdot-12(1+\mu)\left(\frac{\lambda^3+\mu}{1+\mu}\right)^{\frac{2}{3}}\cdot-4(1+\mu)\left(\frac{\lambda^3+\mu}{1+\mu}\right)^{\frac{4}{3}}$

  - $C = \frac{1}{27\lambda^9}+\frac{2}{27\lambda^6}-\frac{3}{5\lambda^5}+\frac{8}{9\lambda^3}-\frac{12}{5\lambda^2}+\frac{9}{\lambda}+24\lambda-18\lambda^2-12\lambda^4-\frac{16\lambda^3\mu}{9(1+\mu)}+\frac{8\lambda^6\mu}{9(1+\mu)}-\frac{(1+\mu)^4}{27(\lambda^3+\mu)^3}-\frac{2(1+\mu)^3}{27(\lambda^3+\mu)^2}-\frac{8(1+\mu)^2}{9(\lambda^3+\mu)}+\frac{9\left(-1+2\lambda^3+\mu\right)}{\left(\frac{\lambda^3+\mu}{1+\mu}\right)^{\frac{1}{3}}}+\frac{3}{5}\left(\frac{\lambda^3+\mu}{1+\mu}\right)^{\frac{1}{3}}\cdot(20\lambda^3-20(2+\mu)+\frac{(1+\mu)^3}{(\lambda^3+\mu)^2}+\frac{4(1+\mu)^2}{\lambda^3+\mu})-\frac{16\mathrm{Log}[\lambda]}{3}+\frac{16}{3}\lambda^3\mathrm{Log}[\lambda]-\frac{-\mu\mathrm{Yeoh}(17+9\mu)+16(1+\mu)\mathrm{Log}[1+\mu]}{9(1+\mu)}+\frac{16}{9}\mathrm{Log}[\lambda^3+\mu]-\frac{16}{9}\lambda^3\mathrm{Log}[\frac{\lambda^3+\mu}{1+\mu}]$

Appendix B: $\lambda\,(\bar{r},\tau)$ Second derivation

Starting with equation (7) we can substitute $\bar{r}_i$ by λ_i to rewrite it as

$$\lambda\,(\bar{r},\tau) \;=\; \sqrt[3]{\frac{(\,{\lambda_i}^3-1\,)}{\bar{R}^3}+1}$$

and derivate with respect to τ (dimensionless time) by applying the chain rule

$$\dot{\lambda} = \frac{1}{3}\left[(\,{\lambda_i}^3-1\,)\frac{{R_i}^3}{R^3}+1\right]^{-2/3}\cdot\; 3\,{\lambda_i}^2\cdot\frac{{R_i}^3}{R^3}\cdot\;\dot{\lambda_\iota}$$

Then, a second derivation can be done to find

$$\ddot{\lambda} = -2\left[(\,{\lambda_i}^3-1\,)\frac{{R_i}^3}{R^3}+1\right]^{-5/3}\cdot\;{\lambda_i}^4\cdot\frac{{R_i}^6}{R^6}\cdot\;\dot{\lambda_\iota}^{\,2}+\left[(\,{\lambda_i}^3-1\,)\frac{{R_i}^3}{R^3}+1\right]^{-2/3}\cdot\;2\,\lambda_i\dot{\lambda_\iota}\frac{{R_i}^3}{R^3}+\ddot{\lambda_\iota}\,{\lambda_i}^2\cdot\frac{{R_i}^3}{R^3}$$

and recalling that

1. $\left[(\,{\lambda_i}^3-1\,)\frac{{R_i}^3}{R^3}+1\right]^{1/3} = \lambda$ and
2. $\frac{{R_i}^3}{R^3} = \frac{\lambda^3-1}{{\lambda_i}^3-1}$

we can finally rearrange terms and obtain

$$\ddot{\lambda} = \frac{\lambda^3-1}{{\lambda_i}^3-1}\left[\frac{2\lambda_i\dot{\lambda_\iota}^{\,2}+{\lambda_i}^2\ddot{\lambda_\iota}}{\lambda^2}-\frac{2{\lambda_i}^4\dot{\lambda_\iota}^{\,2}}{{\lambda_i}^3-1}\frac{\lambda^3-1}{\lambda^5}\right]$$

References

[1] Aranda, D. (2015). "*Constitutive sensitivity of the oscillatory behavior of hyperelastic cylindrical shells".* Master's thesis, Universidad Carlos III de Madrid.

[2] (n.d.). Retrieved February 22, 2016, from

http://www.medicalnewstoday.com/articles/156993.php

[3] Aneurysm: MedlinePlus Medical Encyclopedia. (n.d.). Retrieved February 22, 2016, from https://www.nlm.nih.gov/medlineplus/ency/article/001122.htm

[4] BME 332: Strain/Deformation. (n.d.). Retrieved February 23, 2016, from http://www.umich.edu/~bme332/ch3strain/bme332straindef.htm

[5] Brain (Cerebral) Aneurysm: Symptoms and Signs. (n.d.). Retrieved February 22, 2016, from http://www.medicinenet.com/brain_aneurysm/article.htm

[6] Brain Aneurysm: Causes, Symptoms, Diagnosis, and Treatment - WebMD. (n.d.). Retrieved February 22, 2016, from http://www.webmd.com/brain/tc/brain-aneurysm-topic-overview

[7] MATHEMATICA, Wolfram Res. Inc., Champaign, IL. Available from http://www.wolfram.com

[8] J.K. Knowles, Large amplitude oscillations of a tube of incompressible elastic material. *Quarterly of applied Mathematics 18 (1960) 71-77.*

[9] J.K. Knowles, On a class of oscillations in the finite deformation theory of elasticity, *Journal of Applied Mechanics 29 (1962)* 283-286.

[10] R.W. Ogden, Non-linear Elastic Deformations, *Dover Publications, Mineola, NY, 1997.*

[11] A. Bucchi, E.H. Hearn, Predictions of aneurysm formation in distensible tubes: Part A – '*theoretical background to alternative approaches, International Journal of Mechanical Sciences 71 (2013)* 1-20.

[12] A. Bucchi, E.H. Hearn, Predictions of aneurysm formation in distensible tubes: Part B – application and comparison of alternative approaches, *International Journal of Mechanical Sciences 70 (2013)* 155-170.

[13] M.C. Boyce and Arruda, Constitutive models for rubber elasticity: a review, *Rubber Chemistry and Technology* 73 (2000) 504-523.

[14] A.P.S. Selvadurai, Deflections of a rubber membrane, *Journal of the Mechanics and Physics of Solids* 54 (2006) 1093-1119.

[15] Kelly, Solid mechanics part I. Section 4.3 Volumetric strain. 110-112. Available at

http://homepages.engineering.auckland.ac.nz/~pkel015/SolidMechanicsBooks/Part_I/BookSM_Part_I/04_Strain/04_Strain_03_Volumetric_Strain.pdf

[16] Applied Mechanics of Solids (A.F. Bower) Chapter 3: Constitutive laws - 3.5 Hyperelasticity. (n.d.). Retrieved February 23, 2016, from

http://solidmechanics.org/text/Chapter3_5/Chapter3_5.htm

[17] R.A Canseco de la Cruz, K.A Camarillo Gómez, A. Silva Moreno, R. Lesso Arroyo, *Experimentación y análisis por MEF del Comportamiento Hiperelástico en Materiales usados en Calzado Deportivo,* Ingeniería mecánica, Tecnología y desarrollo Vol 4. No 1 (2011) 023-031.

[18] Dr –Ing. Roland Jakel, PTC. Presentation for the 2nd SAXSIM. Technische Universität Chemnitz 27. April 2010, Rev 1.0

[19] Kelly, Solid mechanics part III. Section 4.4 Isotropic Hyperelasticity. 372-385. Available at http://homepages.engineering.auckland.ac.nz/~pkel015/SolidMechanicsBooks/Part_IV/Chapter_1_Hyperelasticity/PDF/Elasticity_04_Isotropic_Hyperelasticity.pdf

[20] Varas, D. Elasticidad. Universidad Carlos III de Madrid. 2014-2014